Supplementary Information (SI) for RSC Advances.

Supporting Information

A multi-stage computational pipeline and *in vitro* validation for the discovery of small-molecule translation inhibitors targeting the bacterial ribosome

Merve Yuce[1ƚ], Ezgi Koman[2,3 ƚ], Fethiye Aylin Sungur[4], Ayten Karatas[2,3], and Ozge Kurkcuoglu[1]*

[1]Istanbul Technical University, Department of Chemical Engineering, Istanbul, Turkey

[2]Istanbul Technical University, Department of Molecular Biology and Genetics, Istanbul, Turkey

[3]Istanbul Technical University, Molecular Biology-Biotechnology and Genetics Research Center (MOBGAM), Istanbul, Turkey

[4]Istanbul Technical University, Computational Science and Engineering Division, Informatics Institute, Istanbul, Turkey

Corresponding author: olevitas@itu.edu.tr

ƚThese authors have equal contribution.

Molecular Docking to the Peptidyl Transferase Center of the *E. coli* ribosome:

Setting the parameters of Glide / Validation of the Docking Protocol: During the validation step, the docked poses are compared to the native structure ((PDB ID: 4v7v), and the parameters of the calculations that yield a low RMSD were noted. With this purpose, clindamycin was extracted from the clindamycin-bound ribosome structure prepared with the Protein Preparation Wizard implemented in Maestro and re-docked to the binding site by changing/adjusting the default values of the parameters in the software. The 50S large subunit structure (23S rRNA, 5S rRNA, crystal waters, Mg^{2+} ions) in the protein preparation module (Schrodinger Release 2021-4) had a net charge of -2691, and clindamycin was protonated with a charge of +1. Docking studies were performed using Maestro-Glide at standard precision-SP (standard precision) and extra-precision-XP (extra precision) modes.

First, standard precision (SP)-docking calculations were performed and the best pose was determined to be the first pose with the highest score (GlideScore: -9.291 kcal/mol) attained after docking, which had the lowest RMSD value of 0.48 Å compared to the co–crystallized inhibitor. **Figure S1(a)** compares the crystal orientation of the clindamycin molecule in the ribosome structure to the optimal orientation derived from SP-docking calculations. **Figure S1(b)** displays the interactions between 50S and re-docked clindamycin. Hydrogen bonds were primarily responsible for the inhibitor-cavity interactions are dominated by hydrogen interactions involving A2058, G2061, and G2505**,** which are also noted from the crystal structure. In addition, weak interactions between the inhibitor and nucleotides U2504, G2505, U2506 and A2451 are noted. Validation was then conducted with extra precision (XP)-docking using the same parameters as in SP-docking. In **Figure S2(a)**, the best pose for re-docked clindamycin, which had an XP-GlideScore of -11.02 kcal/mol and an RMSD value of 0.77 Å is shown. The interactions of the clindamycin antibiotic with the PTC cavity are displayed in 2D diagram maps using free software Biovia Discovery Studio Visualizer (https://discover.3ds.com/discovery-studio-visualizer-download). Clindamycin exhibited similar interactions as the SP-docking validation pose while maintaining its interactions from the native crystal structure. Several weak interactions were also observed with G2505, A2451 and C2452 nucleotides, electrostatic interactions with U2504 and G2505, as well as hydrogen bonds with A2058, G2061, and G2505 (**Figure S2(b)**). In the calculations employing both SP- and XP-docking, the binding cavity of the inhibitor, its crystal structure pose, and its non-bonding interactions were confirmed. In SP-docking mode, the minimized poses obtained during the docking were ranked using the empirical GlideScore (GScore) function with the following equation,[1]

$$SP\ GlideScore = C_{lipo-lipo}\sum f(r_{lr}) + C_{hbond-neut-neut}\sum g(\Delta r)h(\Delta\alpha) + C_{hbond-neut-charged}\sum g(\Delta r)h(\Delta\alpha) + C_{hbond-charged-charged}\sum g(\Delta r)h(\Delta\alpha) + C_{max-metal-ion}\sum f(r_{lm}) + C_{rotb}H_{rotb} + C_{polar-phob}V_{polar-phob} + C_{coul}E_{coul} + C_{vdW}E_{vdW} + solvation\ terms \quad (1)$$

where C values represent the coefficients, namely the lipophilic-lipophilic, hydrogen bonding (neutral-neutral, neutral-charged and charged-charged donor and acceptor), metal-ion interactions, rotatable bonds, penalty for polar and hydrophobic parts, Coulomb, van der Waals and solvation terms. On the other hand, pose sampling is more comprehensive in XP-docking. It is based on an *anchor-and-grow* strategy. According to this strategy, a part of the molecule is taken from the poses in the SP-docking results and labeled as the *anchor*. Using this *anchor*, new ligand conformations are formed to lower the energy, and this step is called as *grow* [2,3]. Moreover, XP-docking has a different yet improved scoring function, given as,

$$XP\ GlideScore = E_{coul} + E_{vdW} + E_{bind} + E_{penalty} \tag{2}$$

$$E_{bind} = E_{hyd\_enclosure} + E_{hb\_nn\_motif} + E_{hb\_cc\_motif} + E_{PI} + E_{hb\_pair} + E_{phobic\_pair} \tag{3}$$

$$E_{penalty} = E_{desolvation} + E_{ligand\_strain} \tag{4}$$

where E_{coul}, E_{vdW}, E_{bind}, $E_{penalty}$, $E_{hyd\_enclosure}$, $E_{hb\_nn\_motif}$, $E_{hb\_cc\_motif}$, E_{PI}, E_{hb_pair}, E_{phobic_pair}, $E_{desolvation}$ and E_{ligand_strain} represent energy values of Coulomb, van der Waals, binding, penalty, binding hydrophobic enclosure, neutral-neutral hydrogen bonding motifs, charged-charged hydrogen bonding motifs, pi stacking and pi-cation interactions, hydrogen bond, liphophilic pair, desolvation and contact penalties terms.[3] Unlike SP-docking, it has additional terms for desolvation, Coulomb, π-π, π-cation, and van der Waals interactions. Energy optimization is applied to the bond lengths, angles, and torsion angles of the ligand following the docking process; thus, docking poses are improved (Schrödinger Release 2021-4: Glide).

Setting the Parameters of AutoDock Vina. In order to obtain a reliable protocol for docking with AutoDock Vina, the x-ray pose of clindamycin was reproduced by setting the parameters as described in the **Methods**. The RMSD value between the best docking pose and the crystallographic structure was determined as 0.38 Å with a docking score of -8.7 kcal/mol (**Figure S3(a)**). According to docking results, the interactions between the natural inhibitor clindamycin and the binding site involve hydrogen bonding with nucleotides A2058, G2061, and G2505. Additionally, there are electrostatic interactions with nucleotides U2504 and G2505. The interaction pattern observed in the ribosome-clindamycin complex crystal structure was similar to the best re-docking pose having hydrogen bond interactions with A2058, G2061, and G2505. In addition, electrostatic interactions were observed with U2504 and G2505 nucleotides since clindamycin charge is +1. The overlap of the ligand conformations in the best pose and the crystal structure, as well as the similarity of the reproduced inhibitor-nucleotide interactions, confirmed the parameters of the docking protocol (**Figure S3(a)-(b)**).

AutoDock Vina's empirical and knowledge-based scoring function calculates the binding affinity and ranks the binding orientations, which is the sum of the contribution of each weighted energetic factor (Trott & Olson, 2010). The Vina scoring function consists of the sum of the weights of the steric interactions (attractive Gaussian and Repulsion terms), hydrophobic interactions (Hydrophobic) and the hydrogen bonding interactions (Hbond) between the atoms given in the following equations:[4,5]

$$\Delta G_{Binding} = w_1 * Gauss_1(d) + w_2 * Gauss_2(d) + w_R * Repulsion(d) + w_{hp} * Hydrophobic(d) + w_{hb} * Hydrogen\ bonding(d) + w_{rot} * N_{rot} \tag{5}$$

Here *d* is the surface distance calculated as follows:

$$d = r - R_i - R_j \tag{6}$$

where r is the interatomic distance and R_i and R_j are the radii of the atoms in the pair.

Table S1. Molecular docking and Prime MM-GBSA calculations of FDA-approved drug candidates for the peptidyl transferase center.

Drug name / DrugBank ID	Chemical Formula / Molecular Weight (g/mol) / Chemical structure	Chemical class	fragment	XP-GScore / Vina Score (kcal/mol)	Prime MMGBSA $\Delta G_{binding}$ (kcal/mol)	$\Delta G_{\text{binding}}$ (R1, R2, R3) (kcal/mol)
Clindamycin DB01190 (native inhibitor)	$C_{18}H_{33}ClN_2O_5S$ 424.98 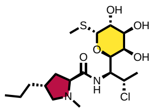	lincosamide antibiotic	**lincosamine ring, pyrrolidine**	-11.3 (SP) -11.5 (XP) -8.9 (vina)	-113.15	-27.47 ± 6.01 -30.51 ± 7.71 -31.85 ± 7.16
Buserelin DB06719	$C_{60}H_{86}$N16O_{13} 1239.45 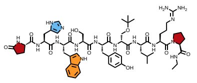	hormones	**indole, imidazole, pyrrolidine**	-12.6 /	-247.87	-52.09 +/- 10.15 -66.76 +/- 13.16 -51.06 +/- 11.28
Cabozantinib DB08875	$C_{28}H_{24}FN_3O_5$ 501.51 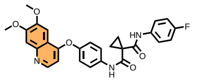	diarylethers	**quinoline**	/ -10.1	-178.15	-47.28 +/- 6.94 -52.42 +/- 7.11 -46.43 +/- 8.77
Daunorubicin DB00694	$C_{27}H_{29}NO_{10}$ 527.52 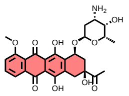	Anthracyc-lines	**anthracycline core**	/ -10.2	-129.79	-20.64 +/- 8.65 -30.13 +/- 11.59 -22.54 +/- 12.09
Elbasvir DB11574	$C_{49}H_{55}N_9O_7$ 882.04 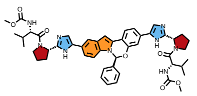	Valine and derivatives	**indole, imidazole, pyrrolidine**	-12.8 /	-207.59	-37.41 +/- 12.12 -42.99 +/- 11.55 -56.26 +/- 12.61
Metocurine DB01336	$C_{40}H_{48}N_2O_6$ 652.82 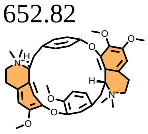	diarylethers	**quinoline**	/ -10.1	-185.6	-42.09 +/- 11.15 -37.01 +/- 10.85 -40.09 +/- 8.72
Mitoxantrone DB01204	$C_{22}H_{28}N_4O_6$ 444.48 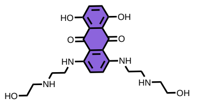	anthraquinon es	**anthraquinone core**	/ -8.6	-173.58	-55.49 +/- 12.77 -41.51 +/- 5.01 -57.98 +/- 16.26
Piperaquine DB13941	$C_{29}H_{32}Cl_2N_6$ 535.52 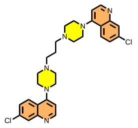	piperazines	**piperazine, quinoline**	-12.0 /	-294.43	-74.11 +/- 5.50 -76.96 +/- 6.80 -99.69 +/- 6.35

Plerixafor DB06809	$C_{28}H_{54}N_8$ 502.78 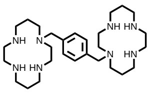	benzenoids	azamacrocycle	-13.7 /	-313.73	-61.19 +/- 6.17 -55.04 +/- 4.85 -54.06 +/- 5.28
Vinblastine DB00570	$C_{46}H_{58}N_4O_9$ 810.97 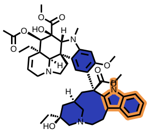	vinca alkaloids	**indole, vinca alkaloid core**	-10.8 /	-221.37	-22.41 +/- 14.07 -26.94 +/- 11.75 -32.01 +/- 11.64
Vinorelbine DB00361	$C_{45}H_{54}N_4O_8$ 778.95 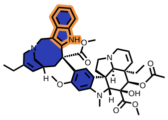	vinca alkaloids	**indole, vinca alkaloid core**	-10.8 /	-191.4	-23.43 +/- 8.76 -20.03 +/- 9.01 -24.52 +/- 7.48

Table S2. Molecular docking and Prime MM-GBSA calculations of Experimental drug candidates for the peptidyl transferase center. Clindamycin is the reference compound.

Drug name / DrugBank ID	**Chemical Formula / Molecular Weight (g/mol) / chemical structure**	**chemical class**	**fragment**	**XP-GScore / Vina Score (kcal/mol)**	**Prime MMGBSA $\Delta G_{binding}$ (kcal/mol)**	**$\Delta G_{binding}$ (R1, R2, R3) (kcal/mol)**
DB01450	$C_{25}H_{35}NO_4$ 413.55 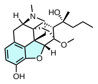	benzoids	coumaran	/ -8.4	-116.43	-22.89 +/- 6.68 -31.29 +/- 6.72 -29.55 +/- 7.48
DB01705	$C_{17}H_{19}N_8$ 335.39 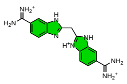	benzimidazol es	benzimidazole	/ -9.6	-159.77	-20.83 +/- 12.33 -17.14 +/- 10.24 -24.21 +/- 10.73
DB01876	$C_{17}H_{14}N_8O$ 346.35 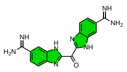	benzimidazol es	benzimidazole	/ -10.1	-154.82	-32.66 +/- 10.99 -35.86 +/- 12.62 -36.90 +/- 10.68
DB02427	$C_{18}H_{21}N_5O_2$ 339.39 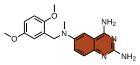	quinazolinam ines	quinazoline	/ -9.2	-137.53	-36.93 +/- 8.46 -21.99 +/- 9.47 -25.77 +/- 6.16
DB02616	$C_{16}H_{15}N_7S_2$ 369.47 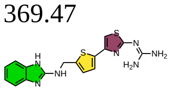	benzimidazol es	benzimidazole , thiophene, thiazole	/ -10.1	-179.34	-30.34 +/- 12.38 -37.52 +/- 16.82 -55.19 +/- 11.08
DB02844	$C_{18}H_{29}N_7O_3S$ 4234.53 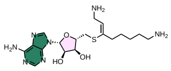	purine nucleoside	adenine, furanose	-11.6 /	-152.64	-23.19 +/- 14.98 -16.42 +/- 10.71 -27.37 +/- 14.14
DB03373	$C_{27}H_{31}N_6O$ 455.58 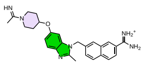	naphthalenes	benzimidazole , piperidine	/ -10.8	-195.68	-46.29 +/- 12.10 -68.14 +/- 7.81 -54.00 +/- 9.54
DB03933	$C_{43}H_{45}ClN_3O_{13}$ 847.28 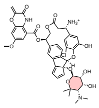	aminoglycosi de	pyranose	/ -11.5	-224.94	-29.13 +/- 12.83 -35.85 +/- 12.21 -58.97 +/- 8.39
DB03986	$C_{11}H_{16}N_5O_4$ 282.28 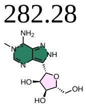	C-glycosyl compounds	adenine, furanose	/ -9.2	-201.23	-41.69 +/- 11.39 -54.26 +/- 6.45 -31.21 +/- 5.52
DB04877	$C_{43}H_{52}N_4O_5$ 704.90 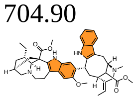	Ibogan-tyoe alkaloids	indole	/ -9.2	-148.21	-23.61 +/- 10.25 -19.32 +/- 12.41 -17.70 +/- 10.40

DB06899	$C_{20}H_{26}N_6O_2S$ 414.52 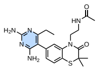	benzothiazines	**pyrimidine**	/ -8.9	-121.41	-41.77 +/- 5.93 -36.64 +/- 10.66 -43.82 +/- 7.13
DB06995	$C_{20}H_{16}F_2N_4O_3$ 398.36 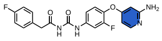	N-acyl-phenylureas	**pyridine**	/ -9.8	-131.09	-45.05 +/- 10.88 -46.97 +/- 6.31 -55.39 +/- 6.33
DB07113	$C_{24}H_{25}F_2N_5O_3$ 469.48 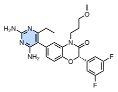	benzoxazinones	**pyrimidine**	/ -9.3	-156.42	-35.83 +/- 7.18 -57.61 +/- 6.55 -32.97 +/- 7.16
DB07618	$C_{24}H_{31}N_5O_2$ 421.54 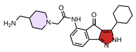	Alpha amino acid amides	**piperidine, pyrazole**	/ -10.6	-140.74	-44.85 +/- 14.75 -43.73 +/- 9.78 -43.94 +/- 9.42
DB07642	$C_{21}H_{24}FN_5O$ 381.45 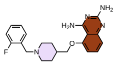	N-benzylpiperidines	**piperidine, quinazoline**	/ -9.5	-178.76	-10.62 +/- 16.95 -45.84 +/- 9.53 -17.06 +/- 11.35
DB07994	$C_{26}H_{23}N_5O$ 421.50 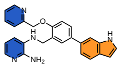	Indoles	**indole, pyridine**	/ -10.0	-144.58	-25.11 +/- 12.15 -39.80 +/- 4.62 -32.42 +/- 7.64
DB08099	$C_{25}H_{31}N_5O$ 417.55 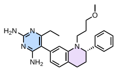	phenylquinolines	**pyrimidine, piperidine**	/ -8.4	-109.75	-40.29 +/- 6.78 -25.54 +/- 11.63 -46.40 +/- 4.59
DB08674	$C_{26}H_{21}N_5O_2$ 435.48 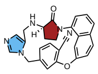	Macrolactams	**imidazole, pyrrolidine**	/ -9.6	-116.79	-33.1 +/- 9.36 -22.64 +/- 6.89 -26.95 +/- 6.65
DB14066	$C_{38}H_{42}N_2O_6$ 622.76 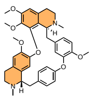	Lignans, diarylethers	**quinoline**	/ -11.0	-163.61	-45.69 +/- 11.49 -50.29 +/- 9.62 -48.00 +/- 7.48

Table S3. Molecular docking and Prime MM-GBSA calculations of Investigational drug candidates for the peptidyl transferase center. Clindamycin is the reference compound.

Drug name / DrugBank ID	**Chemical Formula / Molecular Weight (g/mol) / chemical structure**	**chemical class**	**fragment**	**XP-GScore / Vina Score (kcal/mol)**	**Prime MMGBSA $\Delta G_{binding}$ (kcal/mol)**	**$\Delta G_{binding}$ (R1, R2, R3) (kcal/mol)**
Acarbose DB00284	$C_{25}H_{43}NO_{18}$ 645.61 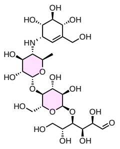	Aminocyclitol glycosides	pyranose	-14.3 /	-159.40	-26.25 +/- 13.93 -36.62 +/- 13.81 -34.68 +/- 12.20
Alvocidib DB03496	$C_{21}H_{20}ClNO_5$ 401.84 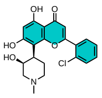	flavones	**flavone core (benzopyrone)**	/ -9.2	-127.00	-33.04 +/- 8.57 -46.47 +/- 5.46 -31.42 +/- 9.06
ATN-161 DB05491	$C_{23}H_{35}N_9O_8S$ 597.65 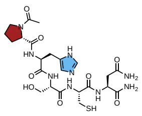	peptides	**imidazole, pyrrolidine**	/ -9.7	-138.98	-29.65 +/- 9.38 -34.99 +/- 11.69 -26.15 +/- 15.27
BMS-214662 DB12234	$C_{25}H_{23}N_5O_2S_2$ 489.61 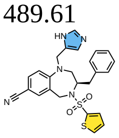	1, 4 benzodiazepin es	**imidazole, thiophene**	/ -9.0	-116.10	-22.07 +/- 11.07 -35.85 +/- 10.62 -32.01 +/- 8.10
Enzastaurin DB06486	$C_{32}H_{29}N_5O_2$ 515.62 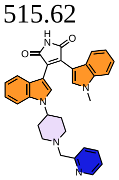	N-alkylindoles	**indole, pyrrolidine, piperidine, pyridine**	/ -11.4	-140.21	-36.83 +/- 5.90 -23.06 +/- 9.53 -24.26 +/- 11.51
GSK-690693 DB12745	$C_{21}H_{27}N_7O_3$ 425.48 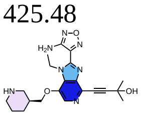	Imidazopyridin es	**imidazole, piperidine, pyridine**	/ -9.7	-130.01	-17.72 +/- 11.65 -23.87 +/- 10.42 -31.00 +/- 12.08
Olcegepant DB04869	$C_{38}H_{47}Br_2N_9O_5$ 869.65 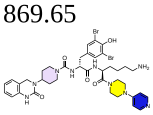	dipeptides	**piperidine, piperazine, pyridine**	-12.7 /	-224.18	-49.87 +/- 12.14 -60.61 +/- 10.92 -60.72 +/- 15.15
Orteronel DB12066	$C_{18}H_{17}N_3O_2$ 307.35 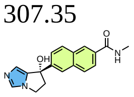	naphthalenecar boxamides	**imidazole, napthalene**	/ -9.1	-127.58	-37.83 +/- 9.14 -47.61 +/- 7.08 -43.11 +/- 7.33

PF-232798 DB14813	$C_{29}H_{40}FN_5O_2$ 509.67 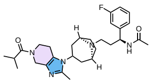	heterocyclic	imidazole, piperidine	/ -10.2	-214.05	-42.08 +/- 10.56 -32.48 +/- 18.40 -49.80 +/- 9.63
Pirarubicin DB11616	$C_{32}H_{37}NO_{12}$ 627.64 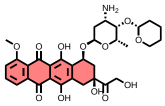	anthracyclines	anthracycline core	-11.5 /	-156.18	-16.97 +/- 56.71 -28.79 +/- 9.42 -17.96 +/- 12.15
Plinabulin DB05992	$C_{19}H_{20}N_4O_2$ 336.40 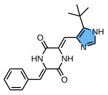	piperazines	imidazole	-11.0 /	-228.94	-78.43 +/- 7.45 -87.83 +/- 9.02 -83.88 +/- 6.65
Ronopterin DB12575	$C_9H_{16}N_6O_2$ 240.26 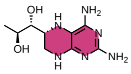	Pteridines and derivatives	pteridine	/ -8.6	-113.85	-25.13 +/- 12.22 -15.68 +/- 8.42 -26.69 +/- 10.94
Ziritaxestat DB15403	$C_{30}H_{33}FN_8O_2S$ 588.71 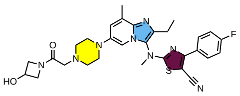	piperazines	piperazine, imidazole, thiazole	/ -11.0	-241.43	-60.86 +/- 11.79 -58.80 +/- 11.36 -55.41 +/- 9.60

Table S4. Optical density measurements at a wavelength of 600 nm (OD_{600}) for the various dilutions of clindamycin incubated with *E. coli* ATCC 10536

Clindamycin concentration (µg/ml)	**128**	**64**	**32**	**16**	**8**	**4**	**2**	**1**	**0.5**
OD_{600}	0.00	0.00	0.00	**0.01**	0.13	0.17	0.71	1.20	1.42
OD_{600}	0.00	0.00	0.00	**0.00**	0.03	0.04	0.78	0.99	1.00
OD_{600}	0.00	0.00	0.00	**0.00**	0.08	0.08	0.68	1.19	1.03
Mean	0.00	0.00	0.00	**0.00**	0.08	0.10	0.73	1.13	1.15
Std. Dev.	0.02	0.01	0.00	**0.01**	0.04	0.06	0.04	0.09	0.19
Clindamycin concentration (µg/ml)	**0.25**	**0.125**	**0.06**	**0.03**	**0.016**	**0.008**	**0.004**	**0.002**	**0**
OD_{600}	1.45	1.46	1.52	1.43	1.48	1.46	1.51	1.50	1.56
OD_{600}	1.17	1.35	1.50	1.43	1.45	1.53	1.55	1.51	1.55
OD_{600}	1.17	1.31	1.54	1.47	1.49	1.35	1.47	1.37	1.56
Mean	1.26	1.37	1.52	1.44	1.47	1.45	1.51	1.46	1.56
Std. Dev.	0.13	0.07	0.02	0.02	0.02	0.07	0.03	0.07	0.01

Table S5. Optical density measurements at a wavelength of 600 nm (OD_{600}) for the various dilutions of mitoxantrone incubated with *E. coli* ATCC 10536

Mitoxantrone concentration (µg/ml)	**128**	**64**	**32**	**16**	**8**	**4**	**2**	**1**	**0.5**
OD_{600}	0.12	**0.08**	0.19	0.21	0.81	1.20	1.53	1.45	1.44
OD_{600}	0.13	**0.11**	0.15	0.17	0.72	1.17	1.33	1.35	1.30
OD_{600}	0.18	**0.09**	0.18	0.16	0.71	1.20	1.32	1.35	1.37
Mean	0.14	**0.09**	0.17	0.18	0.75	1.19	1.39	1.38	1.37
Std. Dev.	0.03	**0.01**	0.02	0.02	0.05	0.01	0.10	0.05	0.06
Mitoxantrone concentration (µg/ml)	**0.25**	**0.125**	**0.06**	**0.03**	**0.016**	**0.008**	**0.004**	**0.002**	**0**
OD_{600}	1.46	1.51	1.60	1.33	1.29	1.24	1.28	1.20	1.17
OD_{600}	1.43	1.41	1.55	1.31	1.25	1.20	1.20	1.23	1.30
OD_{600}	1.33	1.43	1.52	1.32	1.27	1.23	1.25	1.23	1.23
Mean	1.40	1.45	1.56	1.32	1.27	1.22	1.24	1.22	1.24
Std. Dev.	0.06	0.04	0.03	0.01	0.02	0.02	0.03	0.02	0.05

Table S6. Optical density measurements at a wavelength of 600 nm (OD_{600}) for the various dilutions of daunorubicin incubated with *E. coli* ATCC 10536

Daunorubicin concentration (µg/ml)	**128**	**64**	**32**	**16**	**8**	**4**	**2**	**1**	**0.5**
OD_{600}	**0.00**	0.18	0.47	1.33	1.47	1.44	1.32	1.26	1.36
OD_{600}	**0.02**	0.14	0.32	1.26	1.14	1.18	1.15	1.16	1.37
OD_{600}	**0.03**	0.16	0.49	1.21	1.21	1.19	1.48	1.17	1.31
Mean	**0.01**	0.16	0.43	1.27	1.28	1.27	1.31	1.20	1.35
Std. Dev.	**0.01**	0.02	0.07	0.05	0.14	0.12	0.14	0.04	0.02
Daunorubicin concentration (µg/ml)	**0.25**	**0.125**	**0.06**	**0.03**	**0.016**	**0.008**	**0.004**	**0.002**	**0**
OD_{600}	1.38	1.35	1.62	1.51	1.17	1.14	1.41	1.06	1.28
OD_{600}	1.16	1.17	1.24	1.37	1.16	1.15	1.39	1.37	1.13
OD_{600}	1.19	1.30	1.33	1.42	1.52	1.26	1.23	1.23	1.23
Mean	1.24	1.27	1.40	1.43	1.28	1.18	1.35	1.22	1.21
Std. Dev.	0.10	0.07	0.16	0.06	0.16	0.05	0.08	0.12	0.06

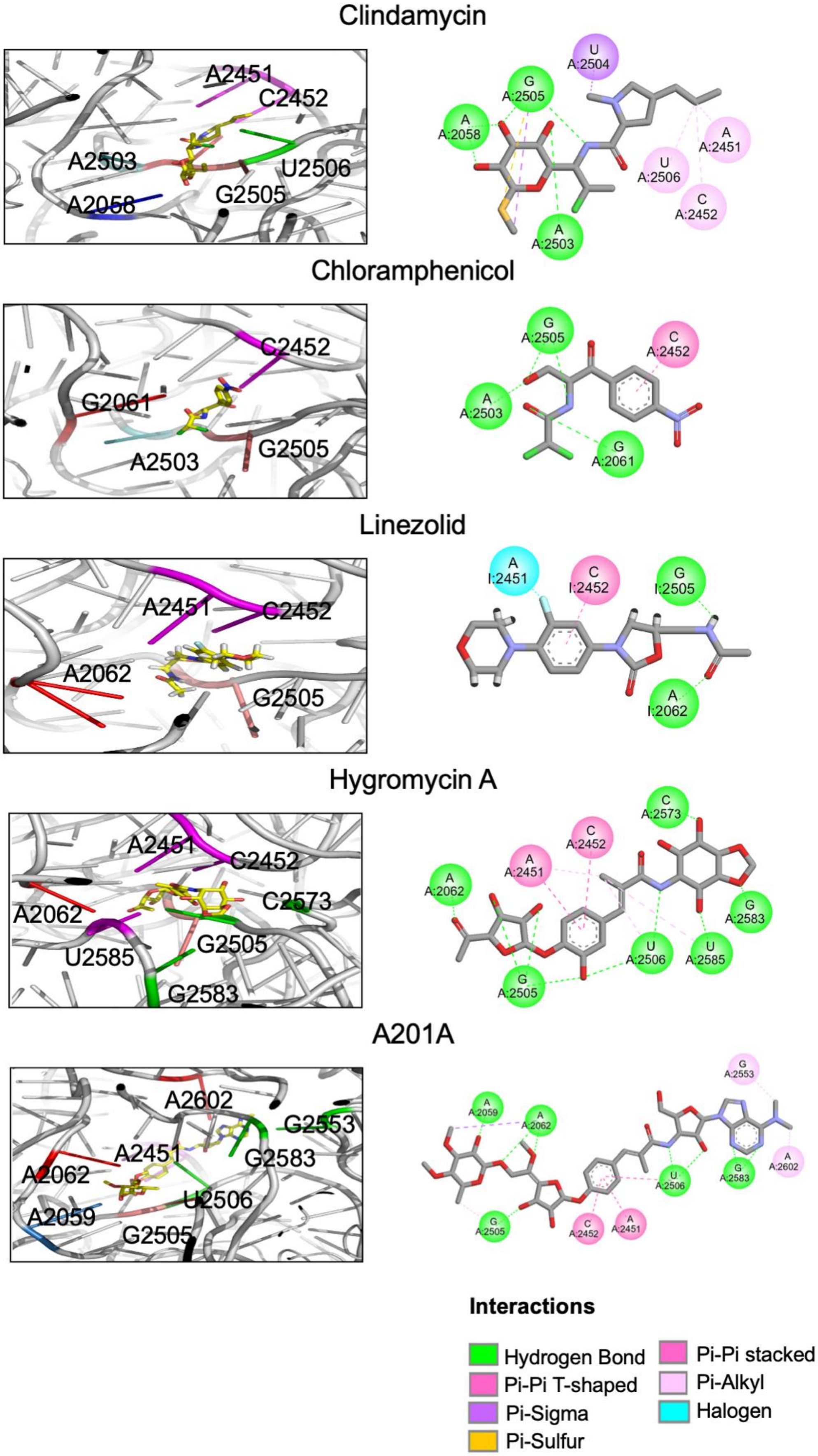

Figure S1. 2D interaction diagrams of known PTC-targeting antibiotics

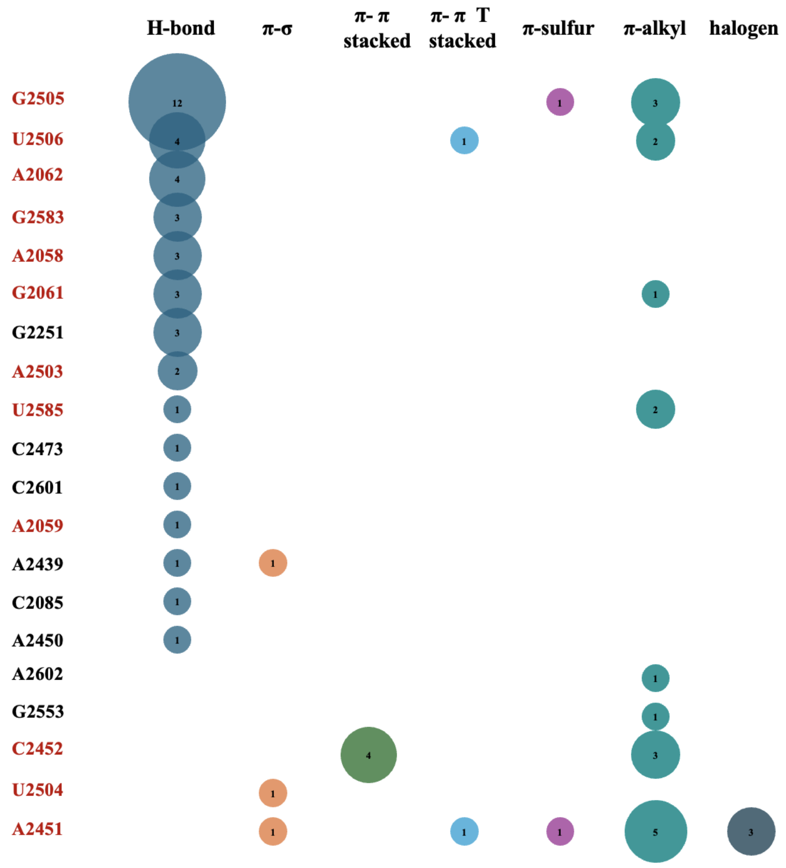

(a)

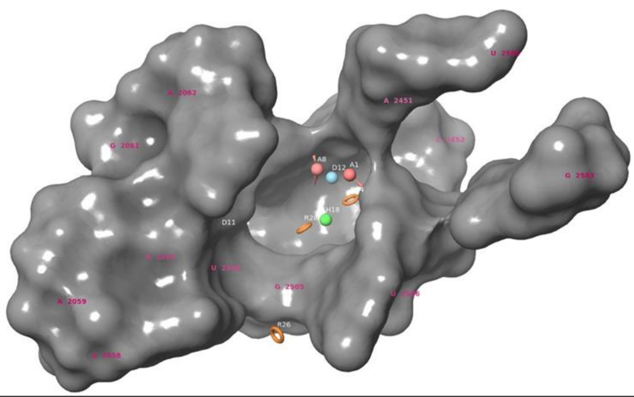

Feature	X	Y	Z	Feature type
H18	-79.50	-57.88	0.47	Hydrophobic
R24	-79.88	-55.77	0.12	Aromatic ring
R28	-76.41	-57.28	1.49	Aromatic ring
R26	-69.61	-59.98	-0.87	Aromatic ring
A8	-79.03	-54.98	3.06	hydrogen bond acceptor
D11	-78.48	-62.97	5.04	hydrogen bond donor
A1	-75.83	-51.78	1.66	hydrogen bond acceptor
D12	-81.28	-56.23	-56.23	hydrogen bond donor

(b)

Figure S2. (a) Number of interactions of PTC-targeting antibiotics **(b)** Pharmacophore hypothesis consisting of 8 features designed for the PTC cavity.

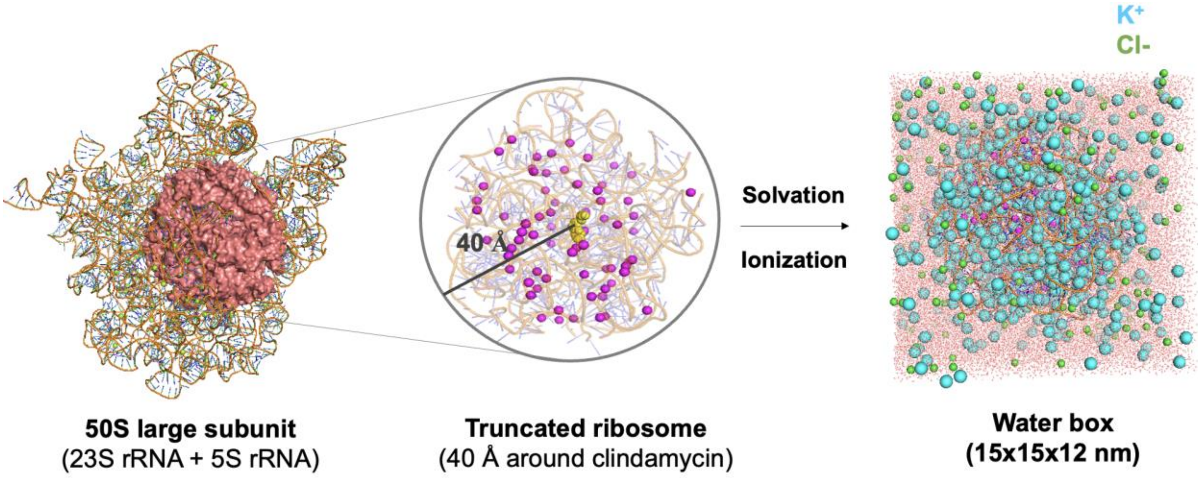

(a)

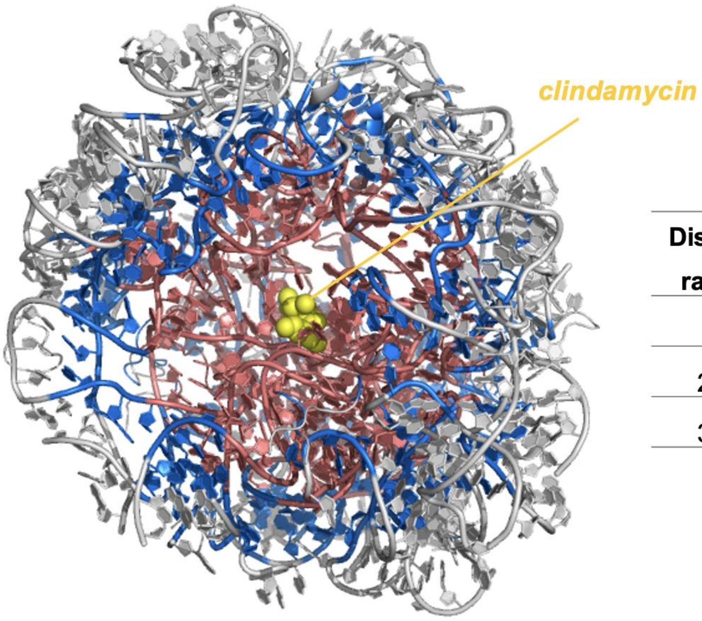

Distance by radius (Å)	Force constant (kcal/mol.Å^2)	# atoms
0 – 24	0	9373
24 – 32	25	8482
32 – 40	50	11332

(b)

Figure S3. (a) MD setup and (b) Harmonic restraint zones on truncated ribosome structure.

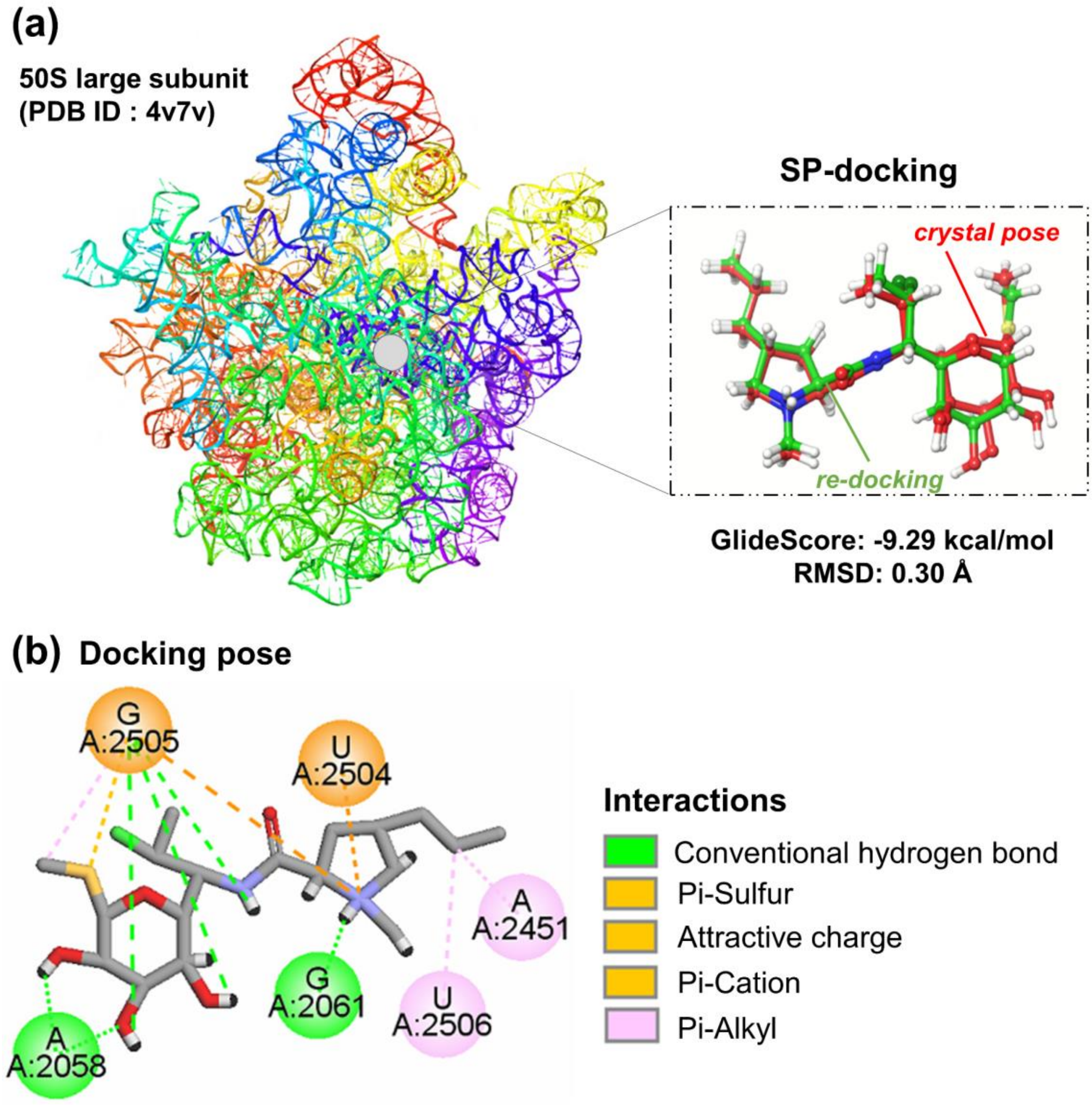

Figure S4. (a) Comparison of the crystal pose and best pose of the native inhibitor Clindamycin derived as a result of SP-docking validation (crystal pose: red, best docking pose: green). **(b)** 2D interaction diagrams for Clindamycin – ribosome interactions. SP-docking best pose is determined by SP-docking validation.

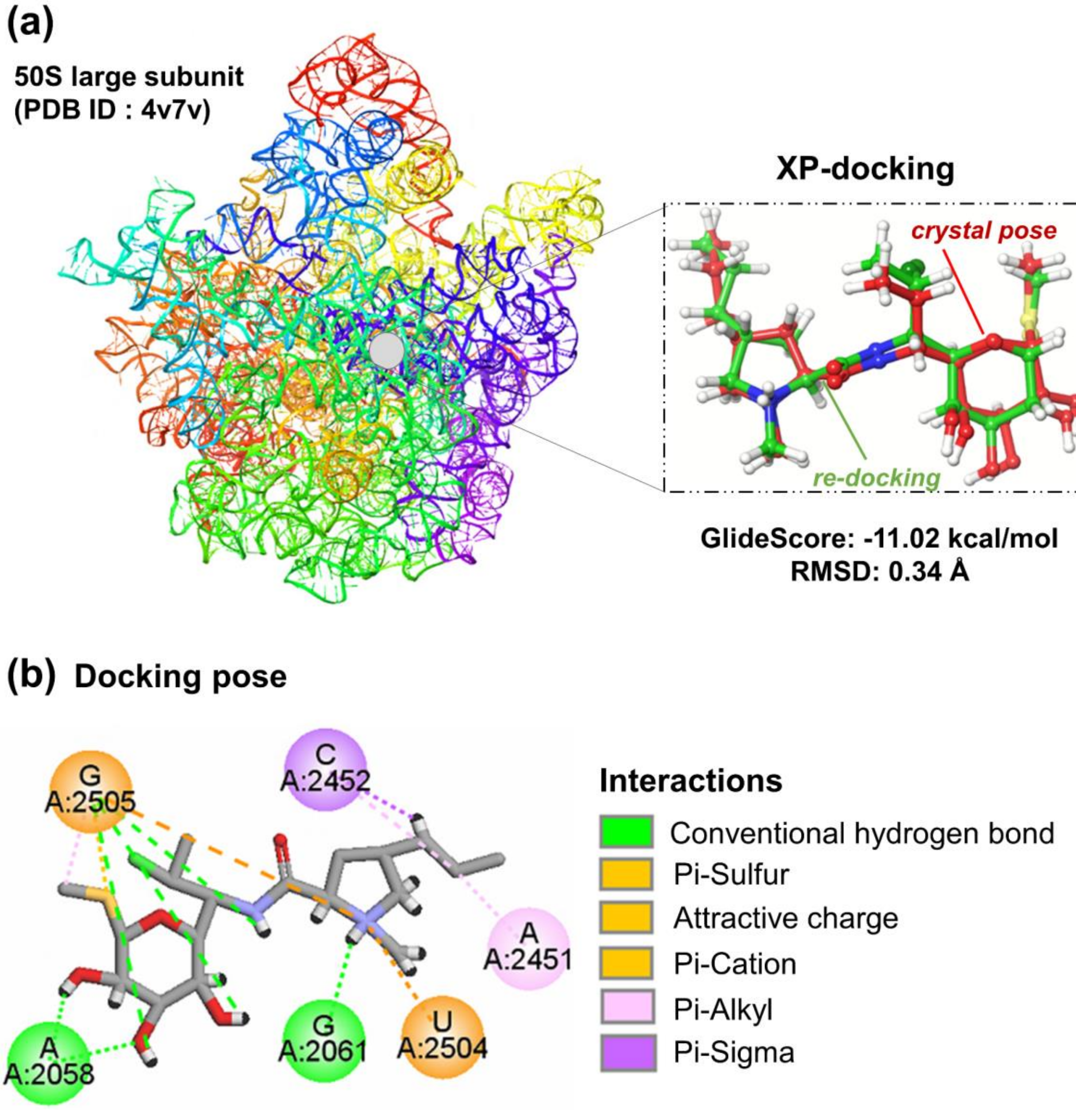

Figure S5. (a) Comparison of the crystal pose and best pose of the native inhibitor Clindamycin derived as a result of XP-docking validation (crystal pose: red, best docking pose: green). **(b)** 2D interaction diagrams for Clindamycin – ribosome interactions. XP-docking best pose is determined by XP-docking validation.

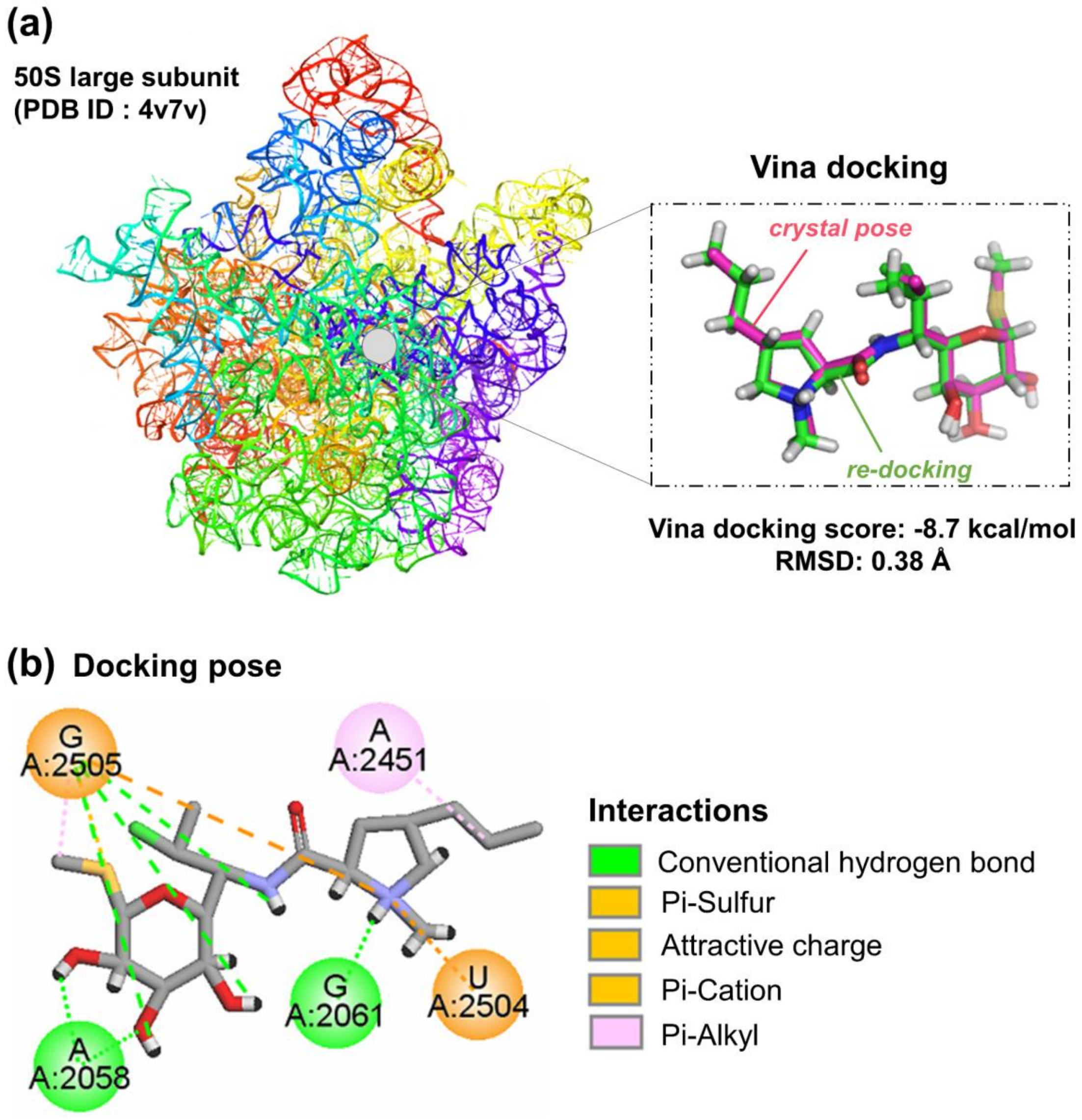

Figure S6. (a) Comparison of the crystal pose and best pose of the native inhibitor Clindamycin derived as a result of AutoDock Vina-docking validation (crystal pose: pink, best docking pose: green) **(b)** 2D interaction diagrams for Clindamycin – ribosome interactions.

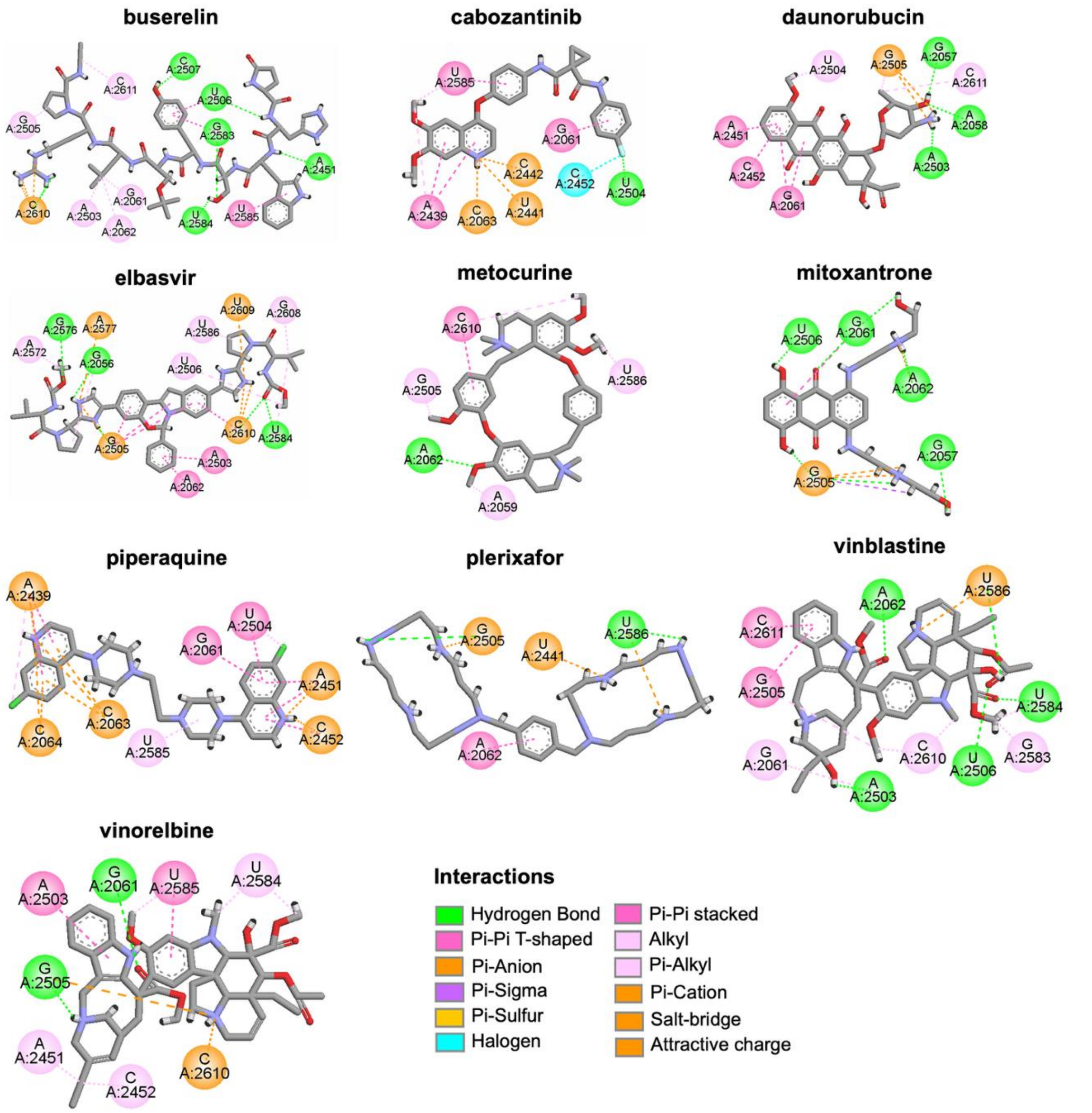

Figure S7. 2D interaction maps for FDA-approved hit compounds obtained from Maestro XP-docking followed by Prime MM-GBSA calculations. Only polar hydrogens are displayed on 2D interaction maps. The non-bonded interactions between the ligand and the surrounding nucleotides based on the color-codes are displayed with dashed lines on 2D maps.

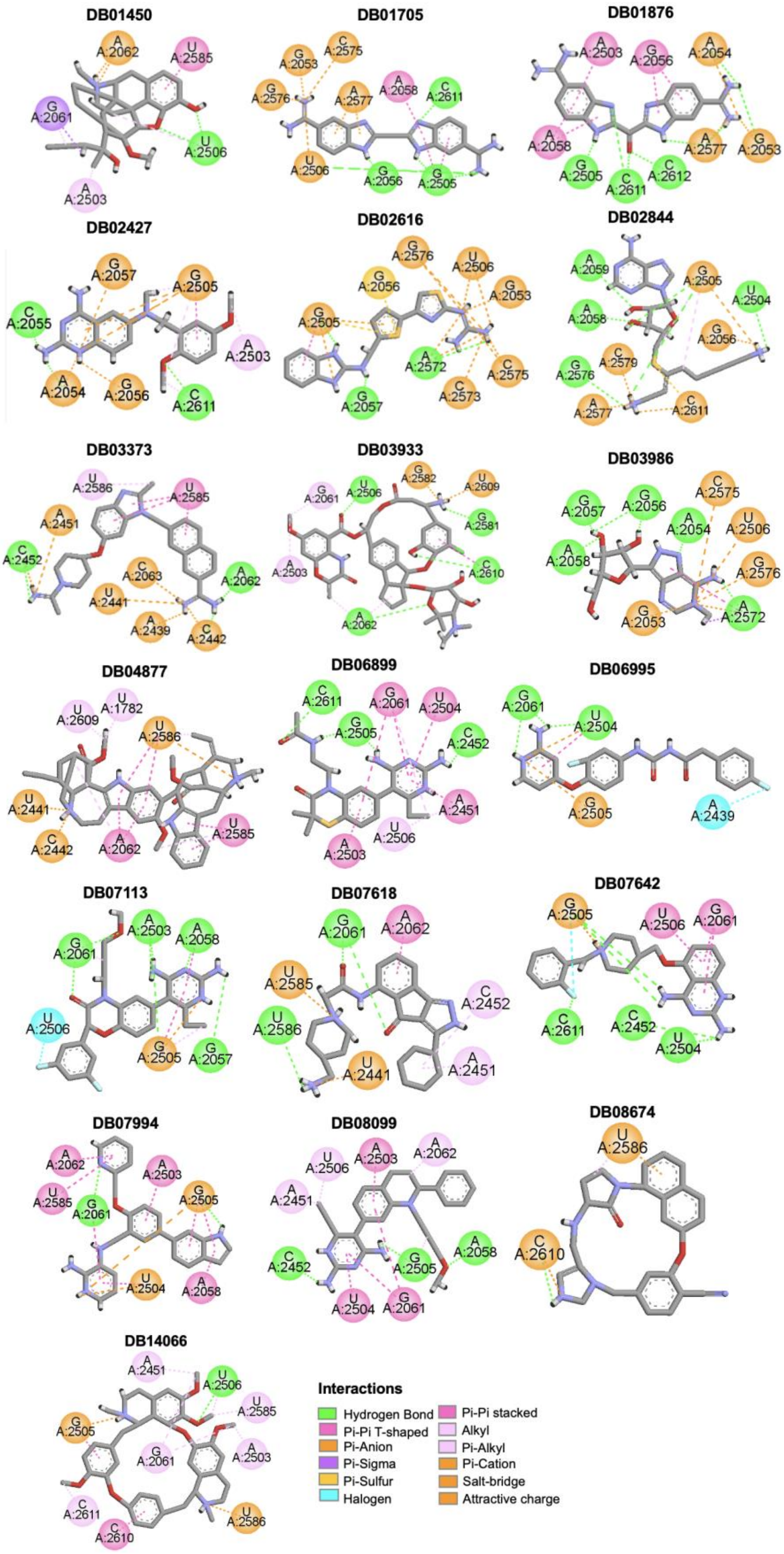

Figure S8. 2D interaction maps for Experimental hit compounds obtained from Maestro XP-docking followed by Prime MM-GBSA calculations. Only polar hydrogens are displayed on 2D interaction maps. The non-bonded interactions between the ligand and the surrounding nucleotides based on the color-codes are displayed with dashed lines on 2D maps.

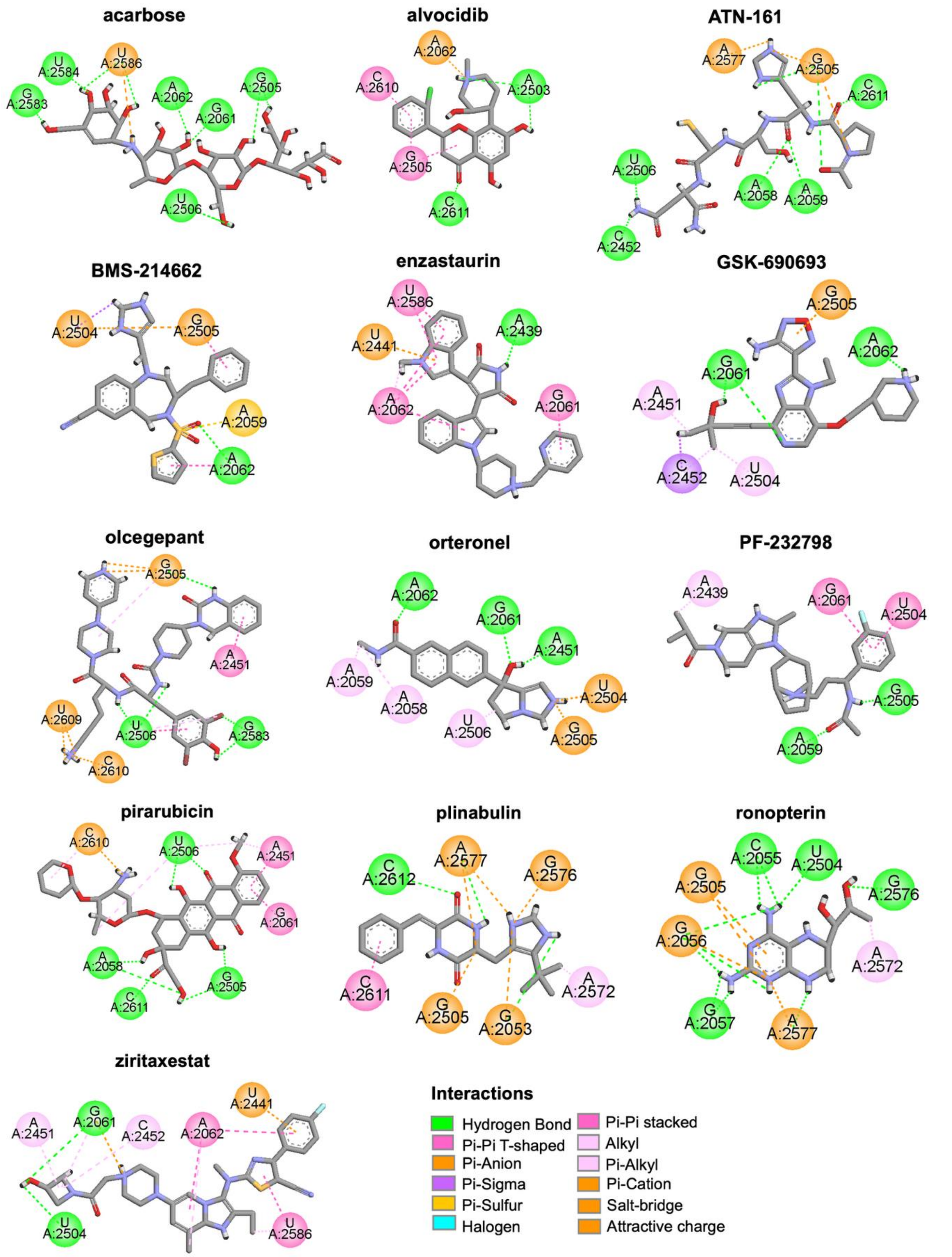

Figure S9. 2D interaction maps for Investigational hit compounds obtained from Maestro XP-docking followed by Prime MM-GBSA calculations. Only polar hydrogens are displayed on 2D interaction maps. The non-bonded interactions between the ligand and the surrounding nucleotides based on the color-codes are displayed with dashed lines on 2D maps.

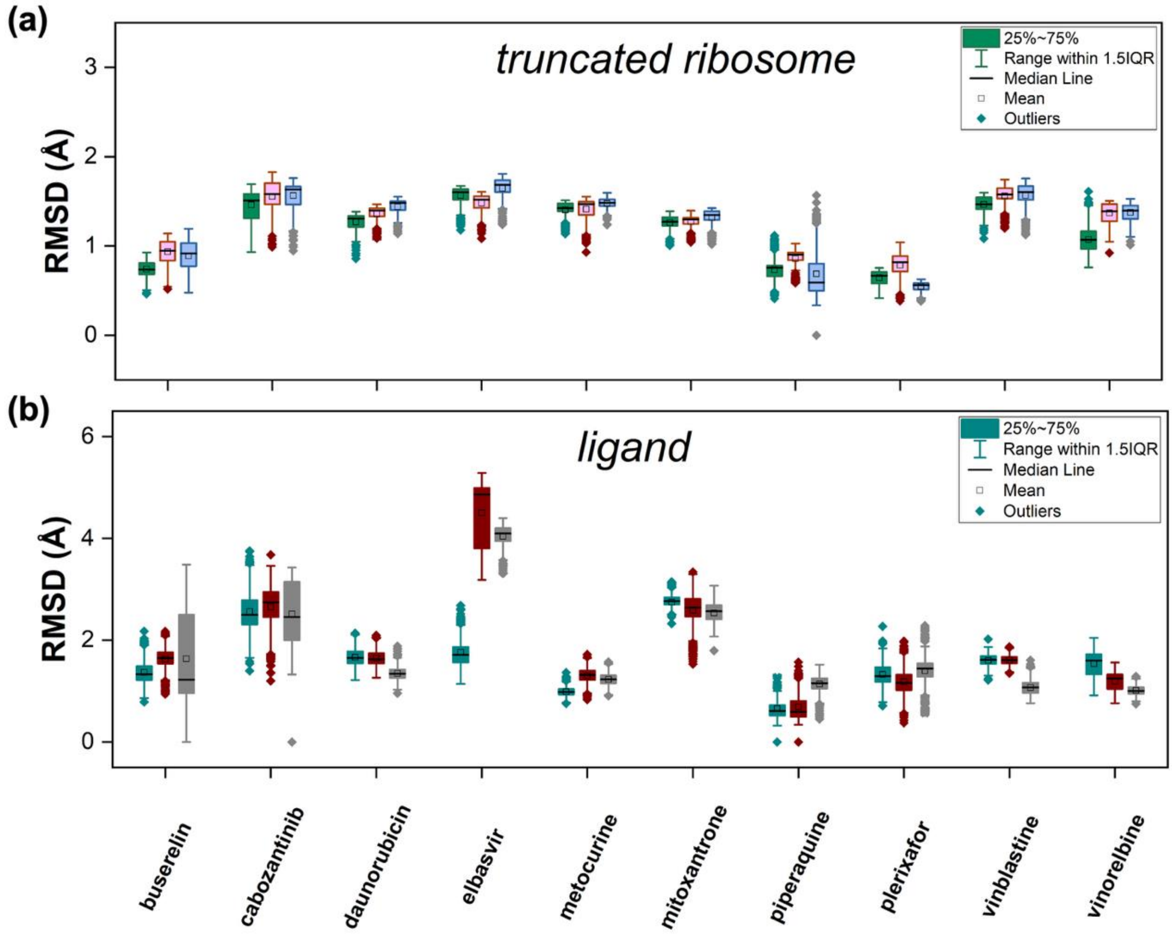

Figure S10. Root mean square deviation (RMSD) on all atoms of **(a)** *E. coli* ribosome and **(b)** FDA-approved hit molecules in 100 ns long MD simulations of 3 replicas.

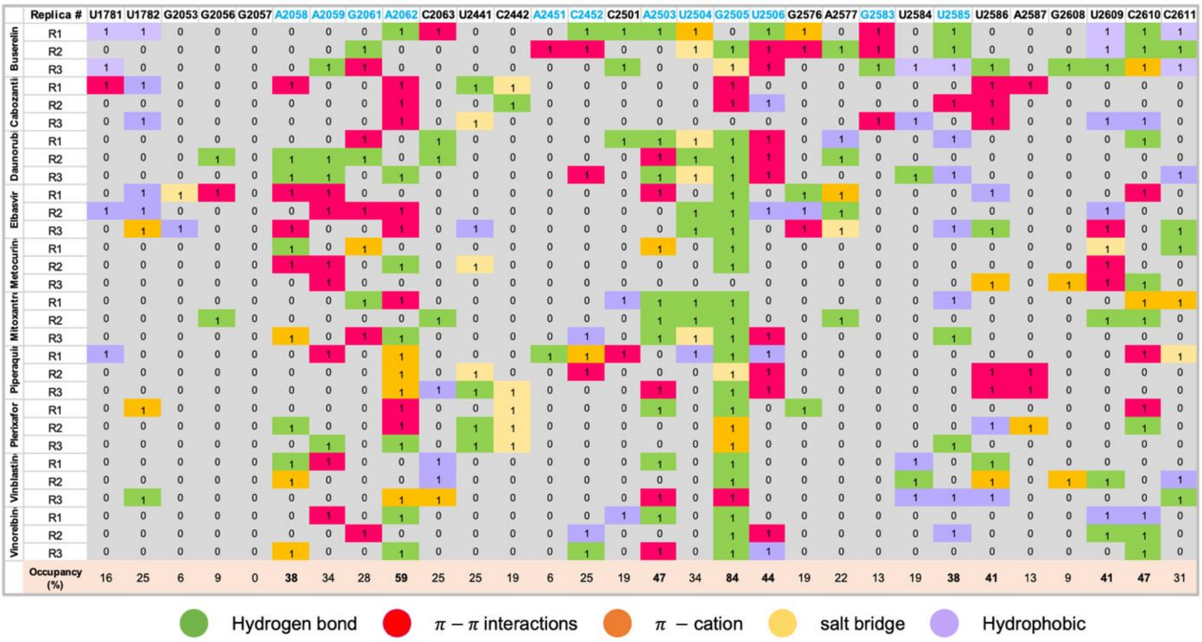

Figure S11. RNA-ligand interaction fingerprinting for selected 10 hit FDA-approved drugs. Residues which have high occurrence in non-bonded interactions with the ligands were indicated at the top and the crystal interactions of the known antibiotics bound to PTC (clindamycin, chloramphenicol, linezolid, hygromycin A and A201A) are displayed in blue. Involvement of the residues in non-bonded interactions were colored according to their hydrogen bond (green), π-π interaction (pink), π-cation (orange), salt-bridge (light orange) and hydrophobic (slate) interactions. Their occurrence percentages indicated at the bottom. Involvement of the residues in non-bonded interactions (observed in more than 10% of 100 ns long production runs) were indicated by 1, whereas their absence is indicated by 0.

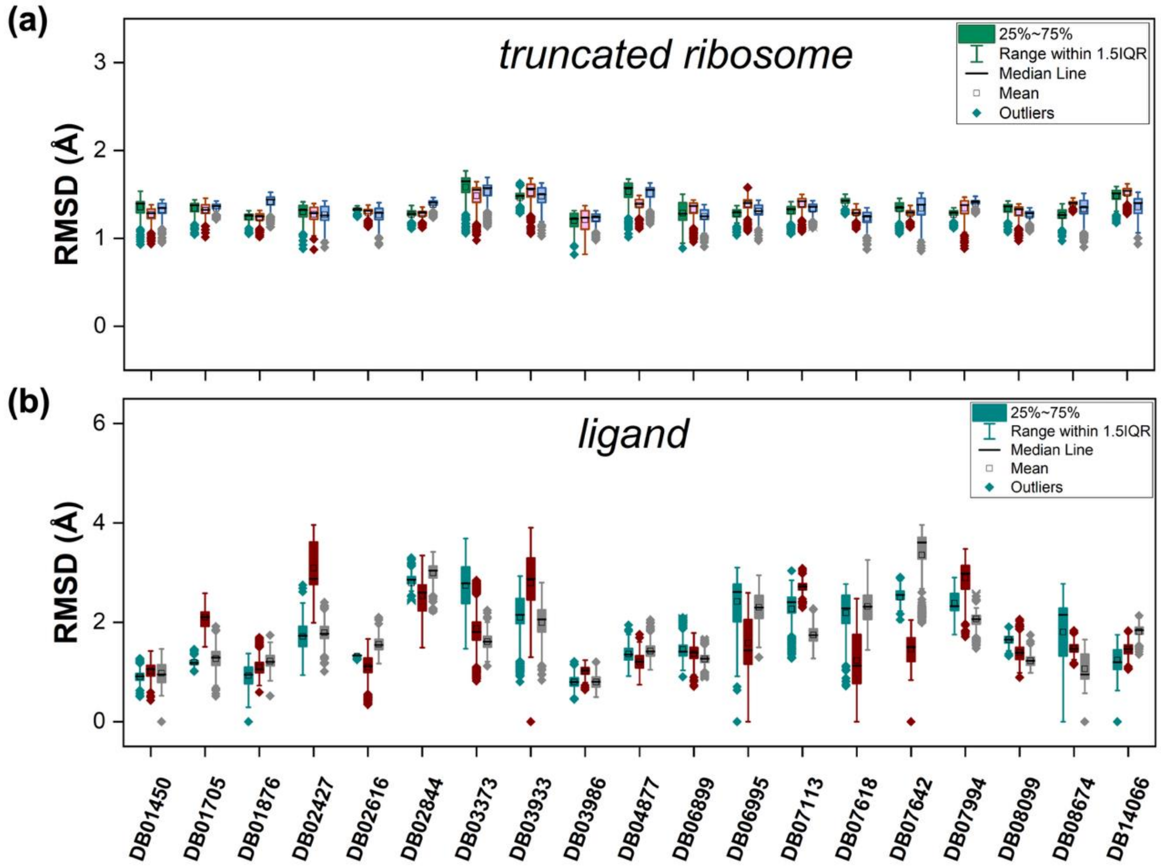

Figure S12. Root mean square deviation (RMSD) on all atoms of **(a)** *E. coli* ribosome and **(b)** Experimental hit molecules in 100 ns MD simulations of 3 replicas.

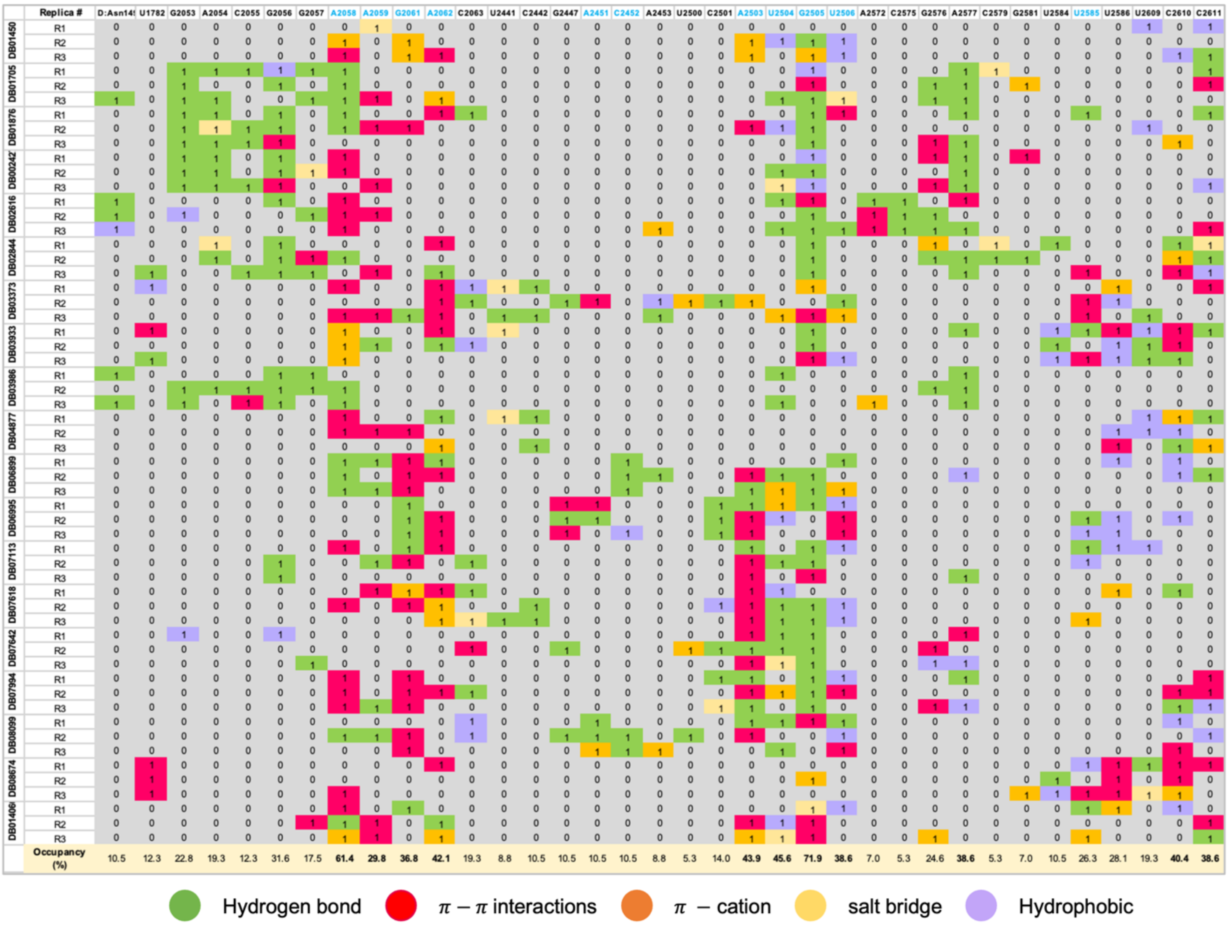

Figure S13. RNA-ligand interaction fingerprinting for selected 19 hit experimental drugs. Residues which have high occurrence in non-bonded interactions with the ligands were indicated at the top and the crystal interactions of the known antibiotics bound to PTC (clindamycin, chloramphenicol, linezolid, hygromycin A and A201A) are displayed in blue. Involvement of the residues in non-bonded interactions were colored according to their hydrogen bond (green), π-π interaction (pink), π-cation (orange), salt-bridge (light orange) and hydrophobic (slate) interactions. Their occurrence percentages indicated at the bottom. Involvement of the residues in non-bonded interactions (observed in more than 10% of 100 ns long production runs) were indicated by 1, whereas their absence is indicated by 0.

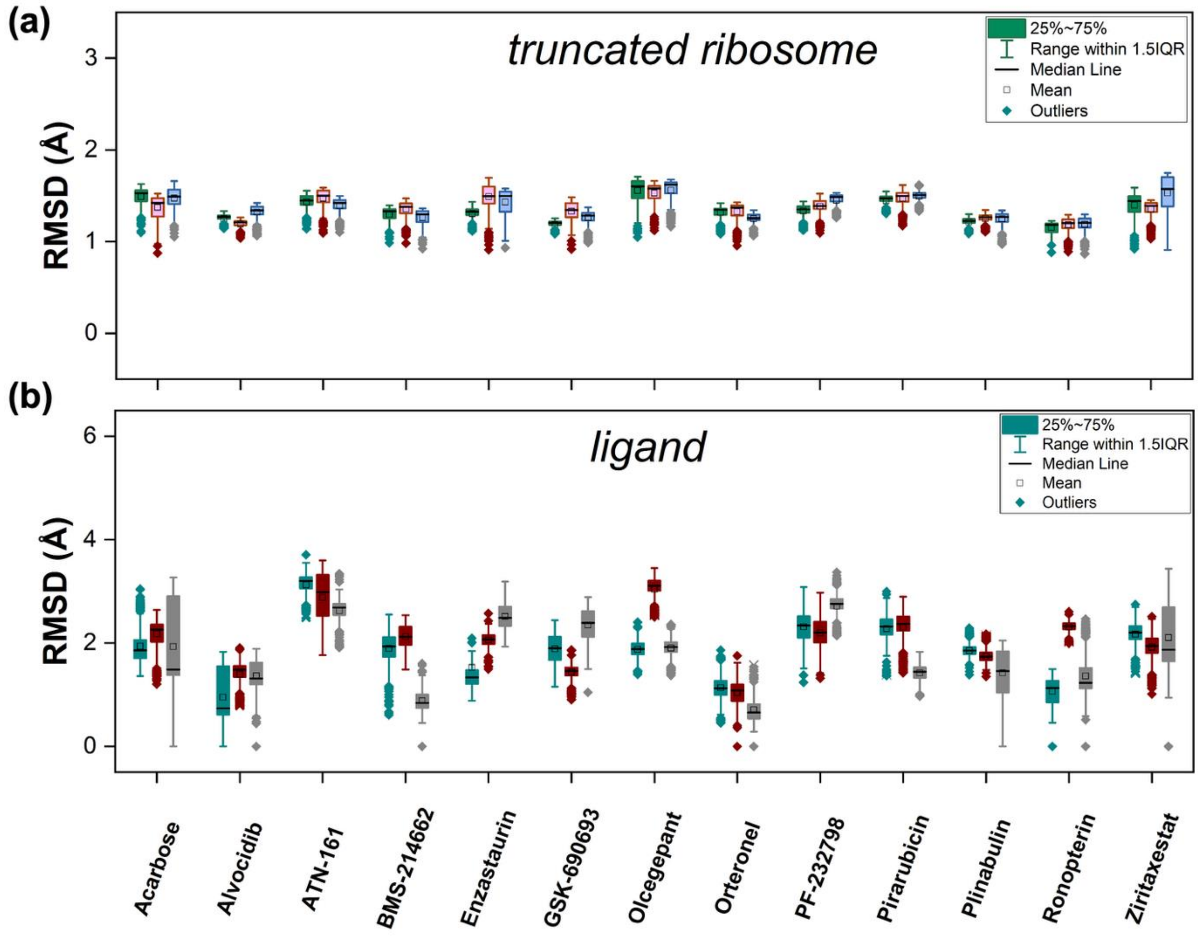

Figure S14. Root mean square deviation (RMSD) on all atoms of **(a)** *E. coli* ribosome and **(b)** Investigational hit molecules in 100 ns MD simulations of 3 replicas.

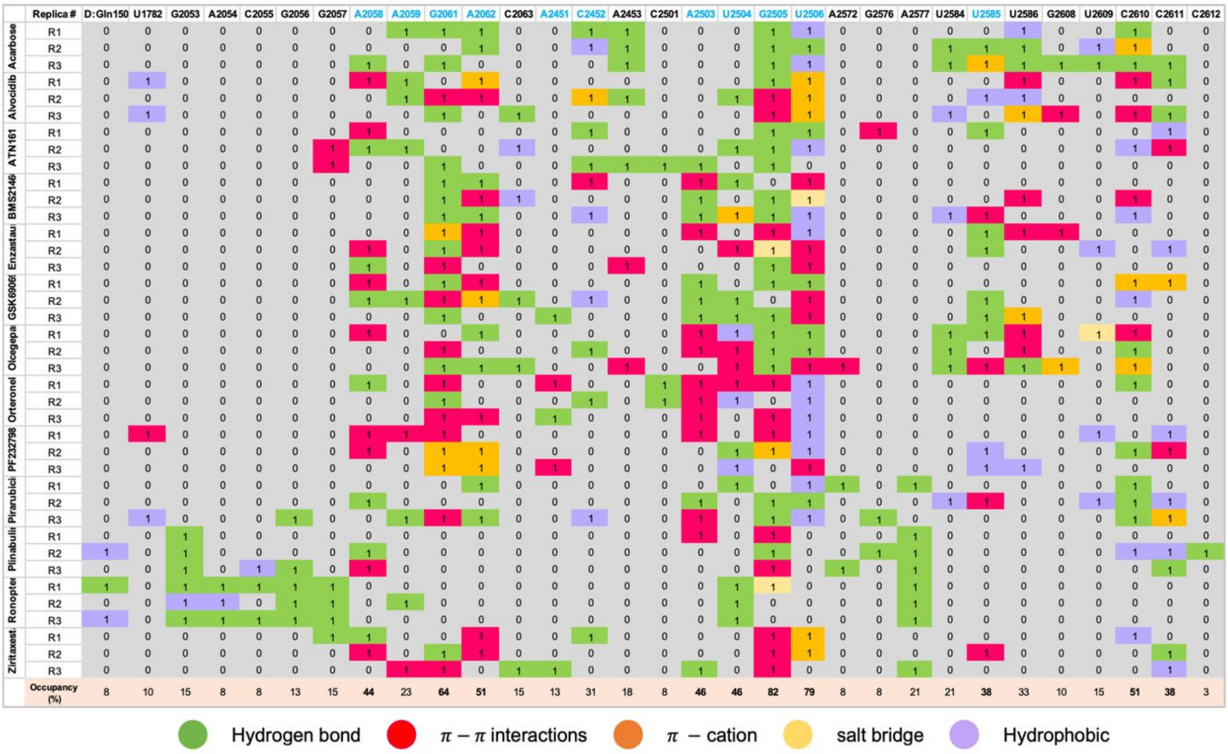

Figure S15. RNA-ligand interaction fingerprinting for selected 13 hit investigational drugs. Residues which have high occurrence in non-bonded interactions with the ligands were indicated at the top and the crystal interactions of the known antibiotics bound to PTC (clindamycin, chloramphenicol, linezolid, hygromycin A and A201A) are displayed in blue. Involvement of the residues in non-bonded interactions were colored according to their hydrogen bond (green), π-π interaction (pink), π-cation (orange), salt-bridge (light orange) and hydrophobic (slate) interactions. Their occurrence percentages indicated at the bottom. Involvement of the residues in non-bonded interactions (observed in more than 10% of 100 ns long production runs) were indicated by 1, whereas their absence is indicated by 0.

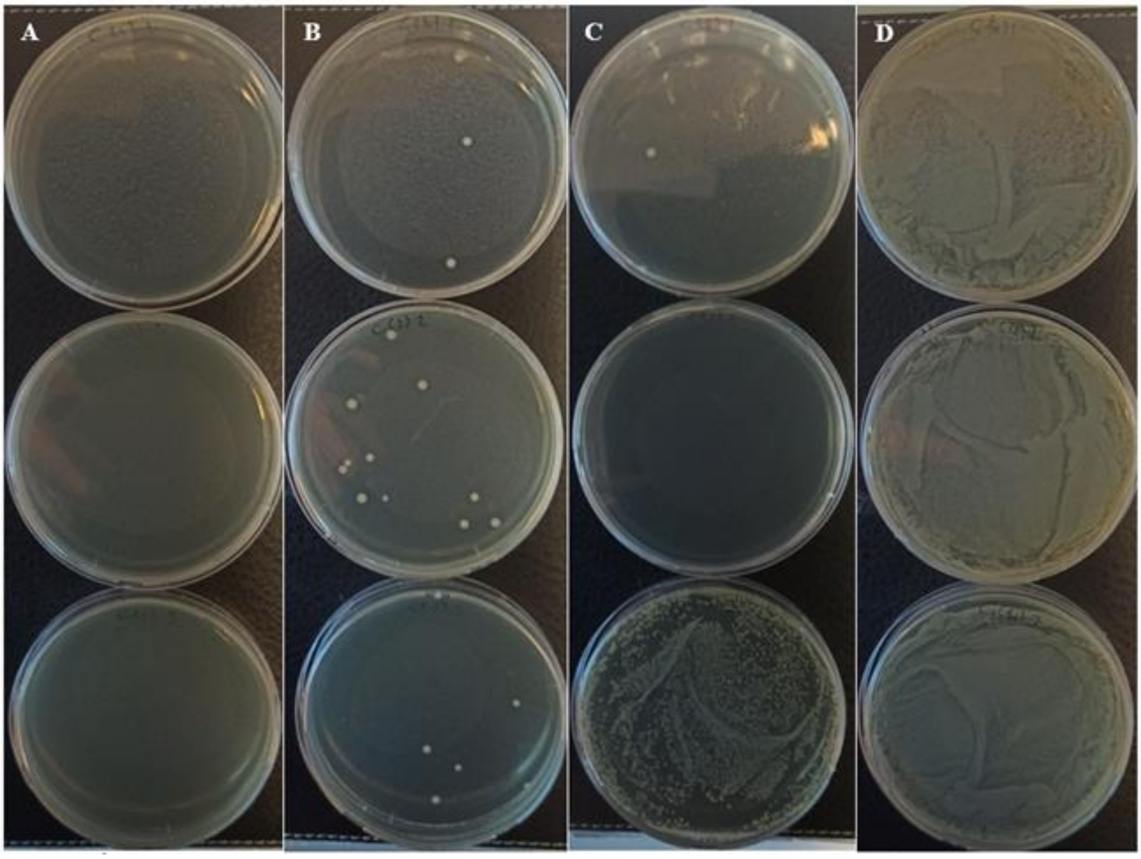

Figure S16. LB agar plates inoculated with samples taken from wells of a 96-well microdilution plate used for MIC testing of clindamycin, containing the following concentrations: (A) 128 µg/ml, (B) 64 µg/ml, (C) 32 µg/ml, and (D) 16 µg/ml clindamycin.

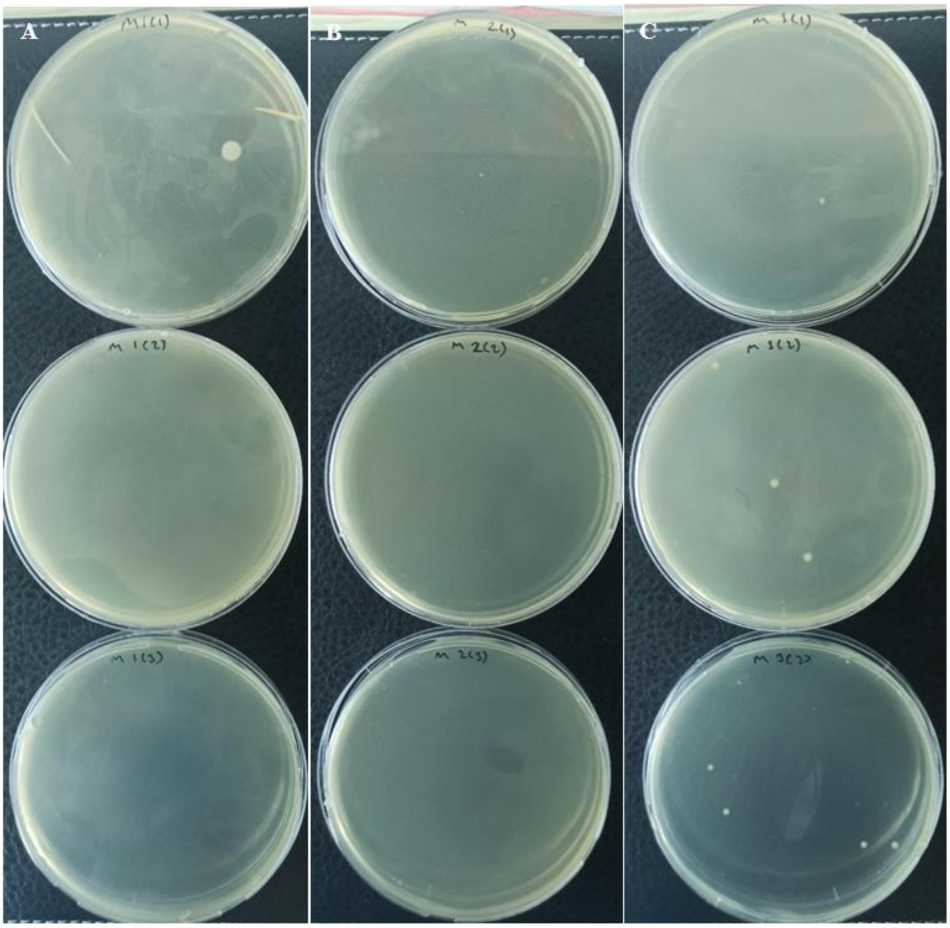

Figure S17. LB agar plates inoculated with samples taken from wells of a 96-well microdilution plate used for MIC testing of mitoxantrone, containing the following concentrations: (A) 128 µg/ml, (B) 64 µg/ml, and (C) 32 µg/ml mitoxantrone.

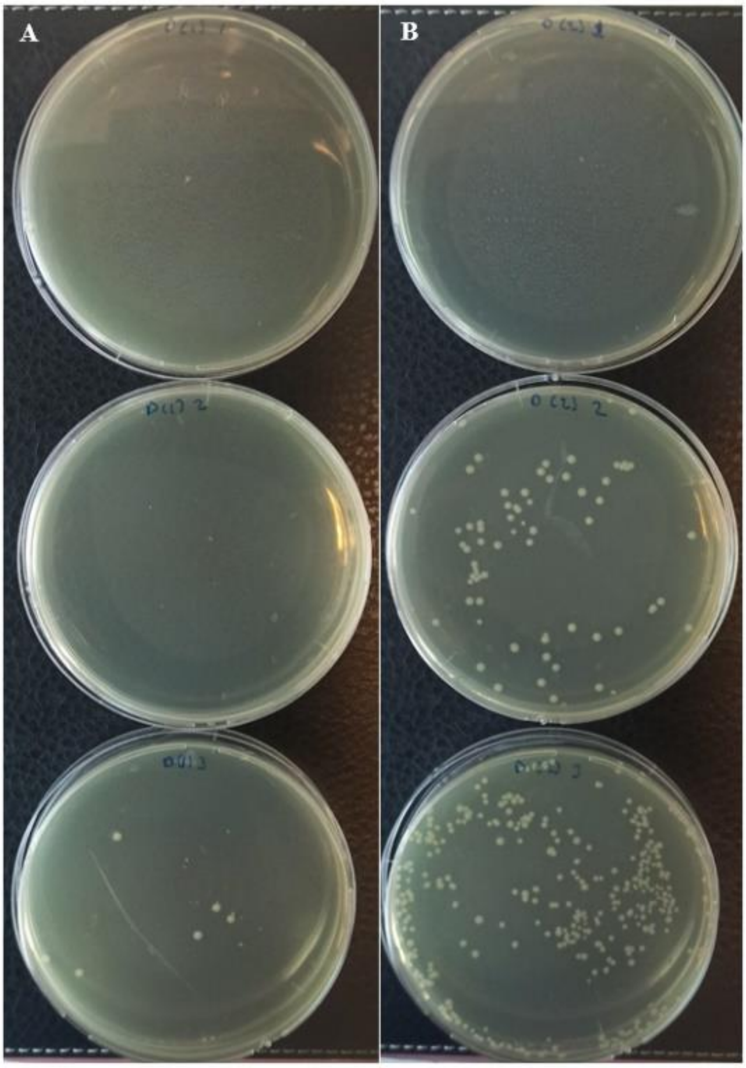

Figure S18. LB agar plates inoculated with samples taken from wells of a 96-well microdilution plate used for MIC testing of daunorubicin, containing the following concentrations: (A) 128 µg/ml, and (B) 64 µg/ml daunorubicin.

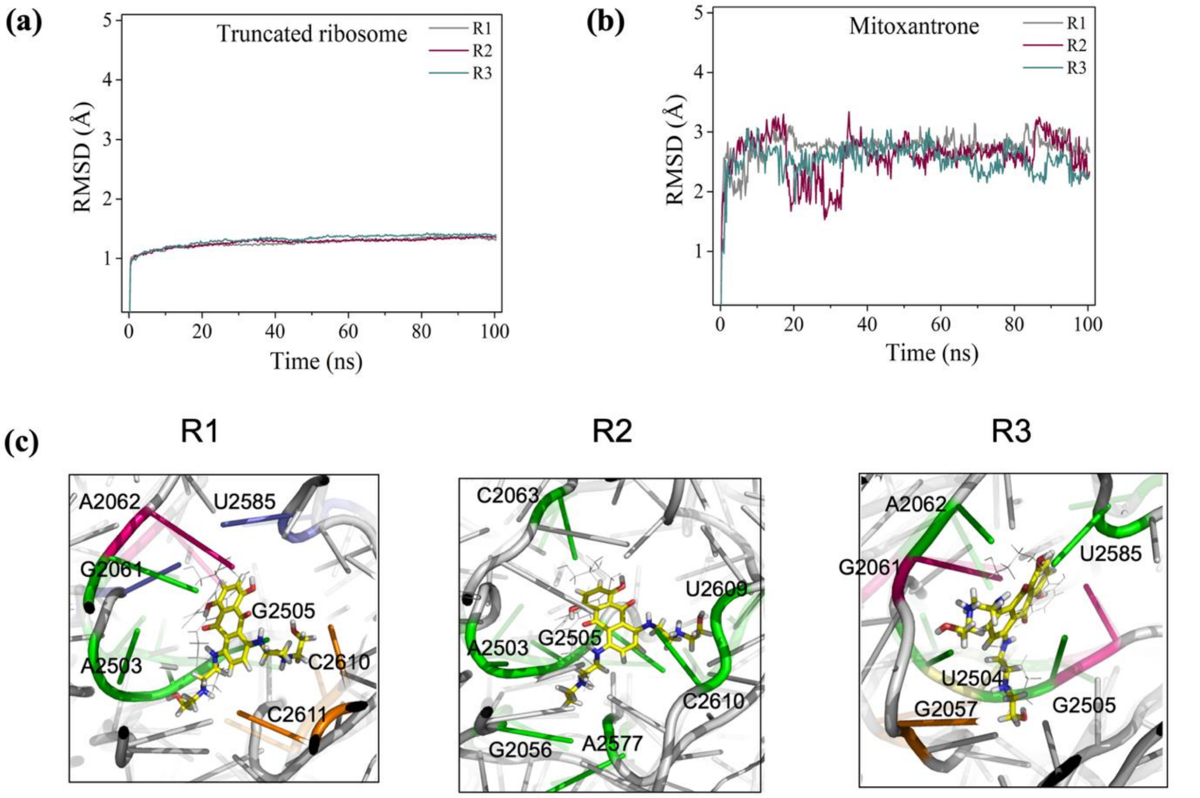

(d)

	Replica #	G2056	A2058	G2061	A2062	C2063	C2452	C2501	A2503	U2504	G2505	U2506	A2577	U2585	U2609	C2610	C2611
Mitoxantrone	R1	0	0	1	1	0	0	1	1	1	1	0	0	1	0	1	1
	R2	1	0	0	0	1	0	0	1	1	1	0	1	0	1	1	0
	R3	0	1	1	1	0	1	0	1	1	1	1	0	1	0	0	0

Hydrogen bond　π - π　π-cation　Salt-bridge　Hydrophobic

Figure S19. RMSD of (a) the truncated ribosomal structure and (b) mitoxantrone from independent MD simulations R1 – R3. (c) Snapshots of the mitoxantrone binding site and non-bonded interactions from R1-R3 simulations. In the snapshots, the frame at 100 ns is highlighted, while the rRNA backbone in the XP-docking pose is transparent, and mitoxantrone is shown in yellow sticks. (e) RNA-ligand interaction fingerprinting for mitoxantrone. Residues that have a high occurrence in non-bonded interactions with the ligand were indicated at the top, and the crystal interactions of the clindamycin are displayed in yellow. The involvement of the residues in non-bonded interactions (observed in more than 10% of 100 ns long production runs) was colored according to their hydrogen bond (green), π-cation (orange), $\pi - \pi$ interactions, hydrophobic (slate), salt-bridge (light orange), and hydrophobic interactions, indicated by 1, whereas their absence is indicated by 0.

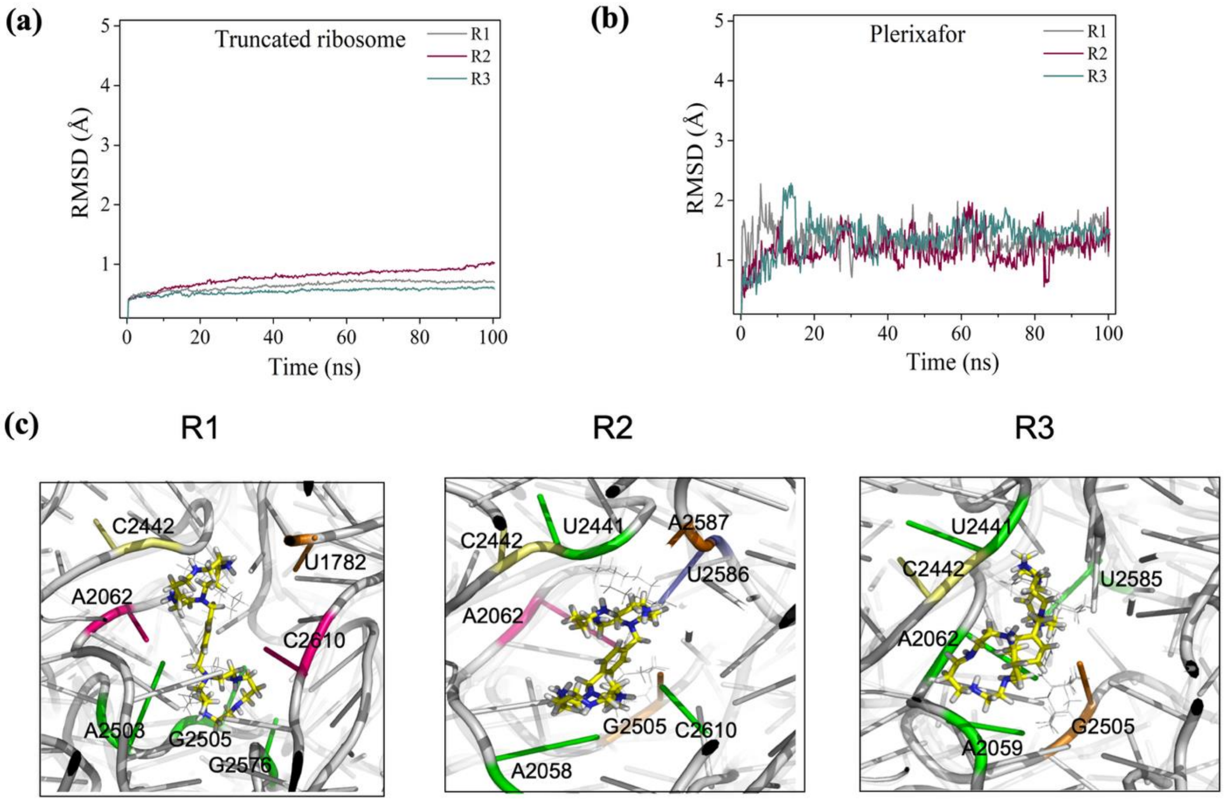

(d)

	Replica #	U1782	A2058	A2059	A2062	U2441	C2442	A2503	G2505	G2576	U2585	U2586	A2587	C2610
Plerixafor	R1	1	0	0	1	0	1	1	1	1	0	0	0	1
	R2	0	1	0	1	1	1	0	1	0	0	1	1	1
	R3	0	0	1	1	1	1	0	1	0	1	0	0	0

Hydrogen bond π - π π-cation   Salt-bridge   Hydrophobic

Figure S20. RMSD of (a) the truncated ribosomal structure and (b) plerixafor from independent MD simulations R1 – R3. (c) Snapshots of the plerixafor binding site and non-bonded interactions from R1-R3 simulations. In the snapshots, the frame at 100 ns is highlighted, while the rRNA backbone in the XP-docking pose is transparent, and plerixafor is shown in yellow sticks. (e) RNA-ligand interaction fingerprinting for plerixafor. Residues that have a high occurrence in non-bonded interactions with the ligand were indicated at the top, and the crystal interactions of the clindamycin are displayed in yellow. The involvement of the residues in non-bonded interactions (observed in more than 10% of 100 ns long production runs) was colored according to their hydrogen bond (green), π-cation (orange), $\pi - \pi$ interactions, hydrophobic (slate), salt-bridge (light orange), and hydrophobic interactions, indicated by 1, whereas their absence is indicated by 0.

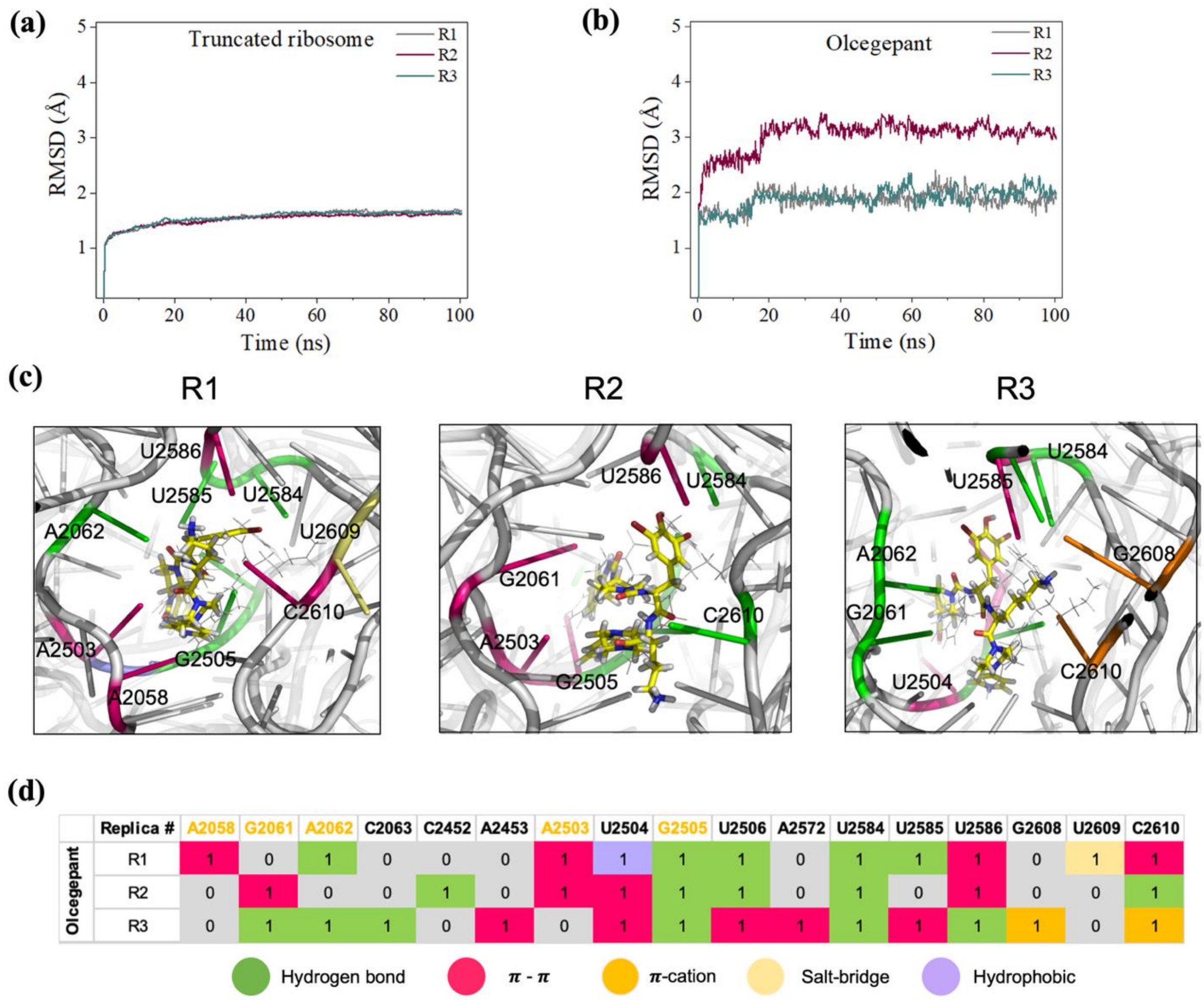

Figure S21. RMSD of (a) the truncated ribosomal structure and (b) olcegepant from independent MD simulations R1 – R3. (c) Snapshots of the olcegepant binding site and non-bonded interactions from R1-R3 simulations. In the snapshots, the frame at 100 ns is highlighted, while the rRNA backbone in the XP-docking pose is transparent, and olcegepant is shown in yellow sticks. (e) RNA-ligand interaction fingerprinting for olcegepant. Residues that have a high occurrence in non-bonded interactions with the ligand were indicated at the top, and the crystal interactions of the clindamycin are displayed in yellow. The involvement of the residues in non-bonded interactions (observed in more than 10% of 100 ns long production runs) was colored according to their hydrogen bond (green), π-cation (orange), $\pi-\pi$ interactions, hydrophobic (slate), salt-bridge (light orange), and hydrophobic interactions, indicated by 1, whereas their absence is indicated by 0.

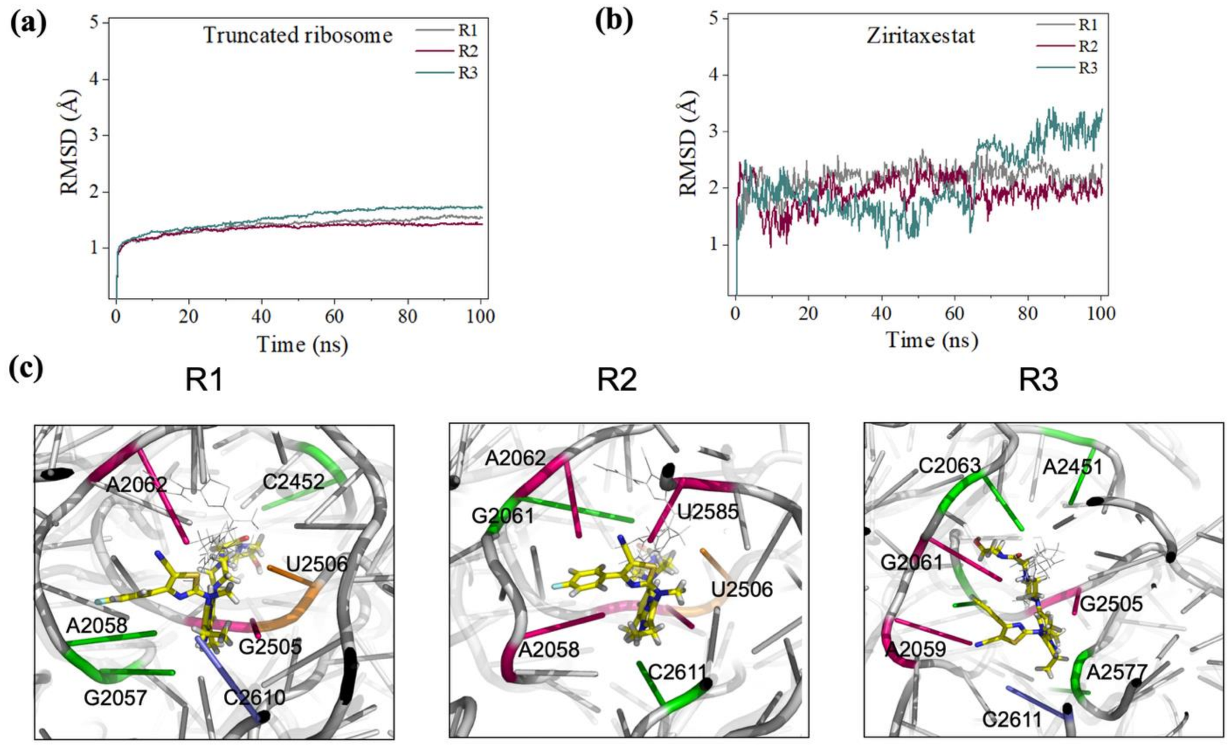

(d)

	Replica #	G2057	A2058	A2059	G2061	A2062	C2063	A2451	C2452	A2503	G2505	U2506	A2577	U2585	C2610	C2611
Ziritaxestat	R1	1	1	0	0	1	0	0	1	0	1	1	0	0	1	0
	R2	0	1	0	1	1	0	0	0	0	1	1	0	1	0	1
	R3	0	0	1	1	0	1	1	0	1	1	0	1	0	0	1

Hydrogen bond π - π π-cation Hydrophobic

Figure S22. RMSD of (a) the truncated ribosomal structure and (b) ziritaxestat from independent MD simulations R1 – R3. (c) Snapshots of the ziritaxestat binding site and non-bonded interactions from R1-R3 simulations. In the snapshots, the frame at 100 ns is highlighted, while the rRNA backbone in the XP-docking pose is transparent, and ziritaxestat is shown in yellow sticks. (e) RNA-ligand interaction fingerprinting for ziritaxestat. Residues that have a high occurrence in non-bonded interactions with the ligand were indicated at the top, and the crystal interactions of the clindamycin are displayed in yellow. The involvement of the residues in non-bonded interactions (observed in more than 10% of 100 ns long production runs) was colored according to their hydrogen bond (green), π-cation (orange), $\pi - \pi$ interactions, hydrophobic (slate), salt-bridge (light orange), and hydrophobic interactions, indicated by 1, whereas their absence is indicated by 0.

REFERENCES

1 R. A. Friesner, J. L. Banks, R. B. Murphy, T. A. Halgren, J. J. Klicic, D. T. Mainz, M. P. Repasky, E. H. Knoll, M. Shelley, J. K. Perry, D. E. Shaw, P. Francis and P. S. Shenkin, *J. Med. Chem.*, 2004, **47**, 1739–1749.

2 M. P. Repasky, M. Shelley and R. A. Friesner, *CP in Bioinformatics*, DOI:10.1002/0471250953.bi0812s18.

3 R. A. Friesner, R. B. Murphy, M. P. Repasky, L. L. Frye, J. R. Greenwood, T. A. Halgren, P. C. Sanschagrin and D. T. Mainz, *J. Med. Chem.*, 2006, **49**, 6177–6196.

4 O. Trott and A. J. Olson, *J Comput Chem*, 2010, **31**, 455–461.

5 R. Quiroga and M. A. Villarreal, *PLoS ONE*, 2016, **11**, e0155183.